# Neogene to Present paleostress field in Eastern Iran (Sistan belt) and implication for regional geodynamics

Michael Jentzer, Marc Fournier, Philippe Agard, Jafar Omrani, Mohammad Mahdi Khatib, Hubert Whitechurch

AGU PUBLICATIONS

Tectonics

RESEARCH ARTICLE
10.1002/2016TC004275

**Key Points:**
- Stress evolution in the Sistan (Eastern Iran) during the Neogene
- Stress transfer throughout Iran during the Neogene
- Zagros collision and stress sources in Iran during the Neogene

**Supporting Information:**
- Supporting Information S1
- Table S1

**Correspondence to:**
M. Jentzer,
michael.jentzer@upmc.fr

**Citation:**
Jentzer, M., M. Fournier, P. Agard, J. Omrani, M. M. Khatib, and H. Whitechurch (2017), Neogene to Present paleostress field in Eastern Iran (Sistan belt) and implications for regional geodynamics, *Tectonics*, *36*, 321–339, doi:10.1002/2016TC004275.

Received 17 JUN 2016
Accepted 3 FEB 2017
Accepted article online 7 FEB 2017
Published online 23 FEB 2017



# Neogene to Present paleostress field in Eastern Iran (Sistan belt) and implications for regional geodynamics

**Michael Jentzer[1], Marc Fournier[1], Philippe Agard[1,2], Jafar Omrani[3], Mohammad Mahdi Khatib[4], and Hubert Whitechurch[5]**

[1]Institut des Sciences de la Terre de Paris, UPMC Université Paris 06, CNRS, Sorbonne Universités, Paris, France, [2]Institut Universitaire de France, Paris, France, [3]Geological Survey of Iran, Tehran, Iran, [4]Department of Geology, University of Birjand, Birjand, Iran, [5]Institut de Physique du Globe, Institut de Géologie, Ecole et Observatoire des Sciences de la Terre, Université de Strasbourg, Strasbourg, France

**Abstract** We conducted a stress field analysis of the northern part of the ~700 km long north-south trending, seismically active Sistan orogenic belt of Eastern Iran formed as a result of the closure of a branch of the Neo-Tethys during the early Cenozoic. Fault kinematic data reveal drastic changes in the stress regime of Eastern Iran during the late Cenozoic, with three successive directions of compression ($\sigma_1$), from 90° N during the middle–late Miocene to 60°N during the late Pliocene and 25°N during the Plio-Quaternary, thereby evidencing a counterclockwise rotation of about 65° of $\sigma_1$ in less than 10 Myr. As shown by compilation of paleostress data, Plio-Quaternary direction of compression in Sistan coincides with the one recorded across the whole of Iran and with present-day Arabia-Eurasia convergence direction. This result suggests effective stress transfer from the Zagros collision and that Sistan is at present mechanically coupled and shortened along with the rest of the Iranian crust/lithosphere. By contrast, Miocene compression is markedly different in the Iranian hinterland (e.g., Sistan, Central Iran, and Kopet Dagh) and in the Zagros orogen. This could tentatively be related to the end of Sistan collision and/or to the imprint of active deformation occurring further to the east. The intermediate late Pliocene compression (i.e., 60°N) could correspond to the progressive reorientation of the stress regime, as Sistan gets mechanically coupled to the Zagros collision.

## 1. Introduction

Characterizing stress regimes and trajectories in the lithosphere is a major challenge in Earth science. Motivation arises from the assessment of geological hazard, as well as from understanding the mechanical behavior of rocks and deciphering tectonic processes at various scales through time. Reconstructing the tectonic history of mountain belts especially requires the knowledge of the successive local and regional directions of shortening through time. Fractures are the most common response of brittlely deformed rocks submitted to tectonic stresses and are therefore classical and reliable indicators of palaeostress/strain patterns in sedimentary rocks.

Progressive closure of the Neo-Tethyan ocean led to the building of numerous mountain belts from the Alps to the Himalayas [*Tapponnier et al*., 1981; *Dercourt et al*., 1986]. In Iran, collision was responsible for the formation of the Zagros and Alborz mountains, buildup of the Iranian plateau and further inland, in eastern Iran, for the formation of the Sistan moutain belt (Figure 1) [*Stöcklin*, 1968; *Tirrul et al*., 1983; *Agard et al*., 2011].

The Sistan belt stretches N-S along ~700 km at a high angle to adjacent mountain belts (Figure 1). It is characterized by a wealth of preserved Mesozoic ophiolites [*Saccani et al*., 2010; *Zarrinkoub et al*., 2012], large-scale Cenozoic basins [*Tirrul et al*., 1983], profuse Cenozoic magmatism [*Camp and Griffis*, 1982; *Pang et al*., 2012, 2013], and varied metamorphic rocks, including high-pressure low-temperature relicts (HP-LT) [*Fotoohi Rad et al*., 2005; *Angiboust et al*., 2013; *Bröcker et al*., 2013]. The Sistan belt results from the closure of a small oceanic branch of the Neo-Tethys ocean during the Cenozoic.

The tectonic and geodynamic evolution of Sistan was little studied, except for pioneering geological studies across the "Sistan suture zone" dedicated to regional mapping [*Freund*, 1970; *Tirrul et al*., 1983]. More recent studies mainly focus on active tectonics, deformation rates, and seismic hazard assessment [*Berberian et al*., 1999, 2000; *Vernant et al*., 2004; *Walker and Jackson*, 2004; *Walker and Khatib*, 2006;

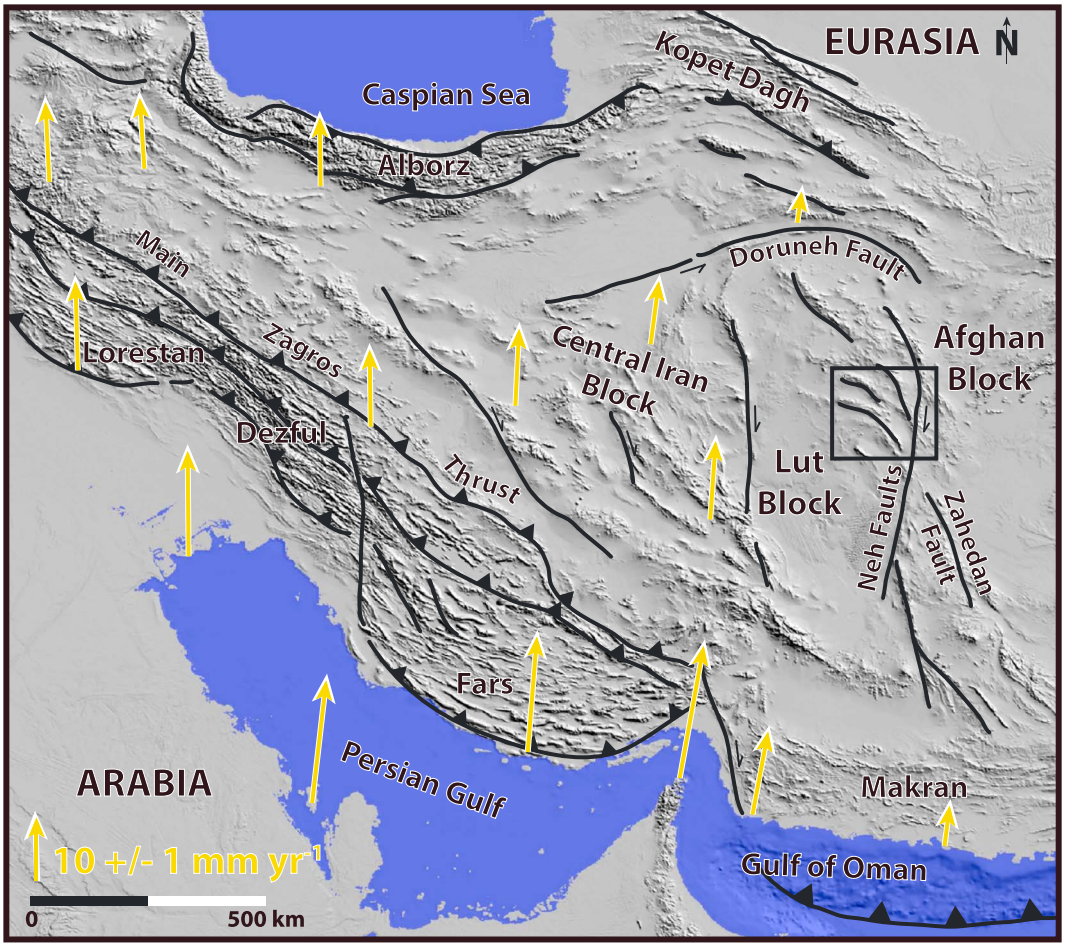


**Figure 1.** Location of the north Sistan orogenic belt (black square) and main Iranian belts. The Zagros belt is made up of the Lorestand, Dezful, and Fars provinces. Arrows show GPS motions relative to stable Eurasia [*Vernant et al*., 2004].

*Farbod et al*., 2016]. The purpose of the present paper is to provide constraints on the stress field evolution in the Sistan belt during the late Cenozoic. Paleostress fields are established by inversion of fault slip data sets in sedimentary rocks. Our study supplements for a key region, the eastern part of Iran, the tectonic evolution previously established with the same method in the Zagros and Makran mountains. The compilation of Iranian paleostress studies allows us to propose a model of intraplate stress transfer throughout the Iranian crust during the Cenozoic. Unlike the Zagros, however, little is known about the paleostress field in this region and its evolution through time.

## 2. Geological Setting

### 2.1. Overall Architecture of the Sistan Belt

The Sistan belt was mapped in 1977 and 1978 at 1:50,000 scale, as a part of an extensive regional mapping and mineral exploration program undertaken by the Geological and Mineral Survey of Iran. The main observations and conclusions were published in *Tirrul et al.* [1983], and only the main conclusions are recalled here. Based on lithostratigraphic and structural studies and age determinations, these authors suggested that the belt could be divided into five main units (Figure 2): The (1) Lut and (2) Afghan continental blocks, where Neoproterozoic to Paleozoic basement and granulite facies metamorphic rocks are exposed [*Stöcklin*, 1968; *Nadimi*, 2007; *Bagheri and Stampfli*, 2008]. On top of this basement, Jurassic series and Cretaceous Orbitolina limestones (Barremian to Aptian) were deposited. These sedimentary rocks are mildly affected by deformation occurring during the Sistan belt formation. The (3) Neh Complex comprises weakly metamorphosed ophiolites and ophiolitic mélanges together with low-grade metasedimentary rocks of Senonian to

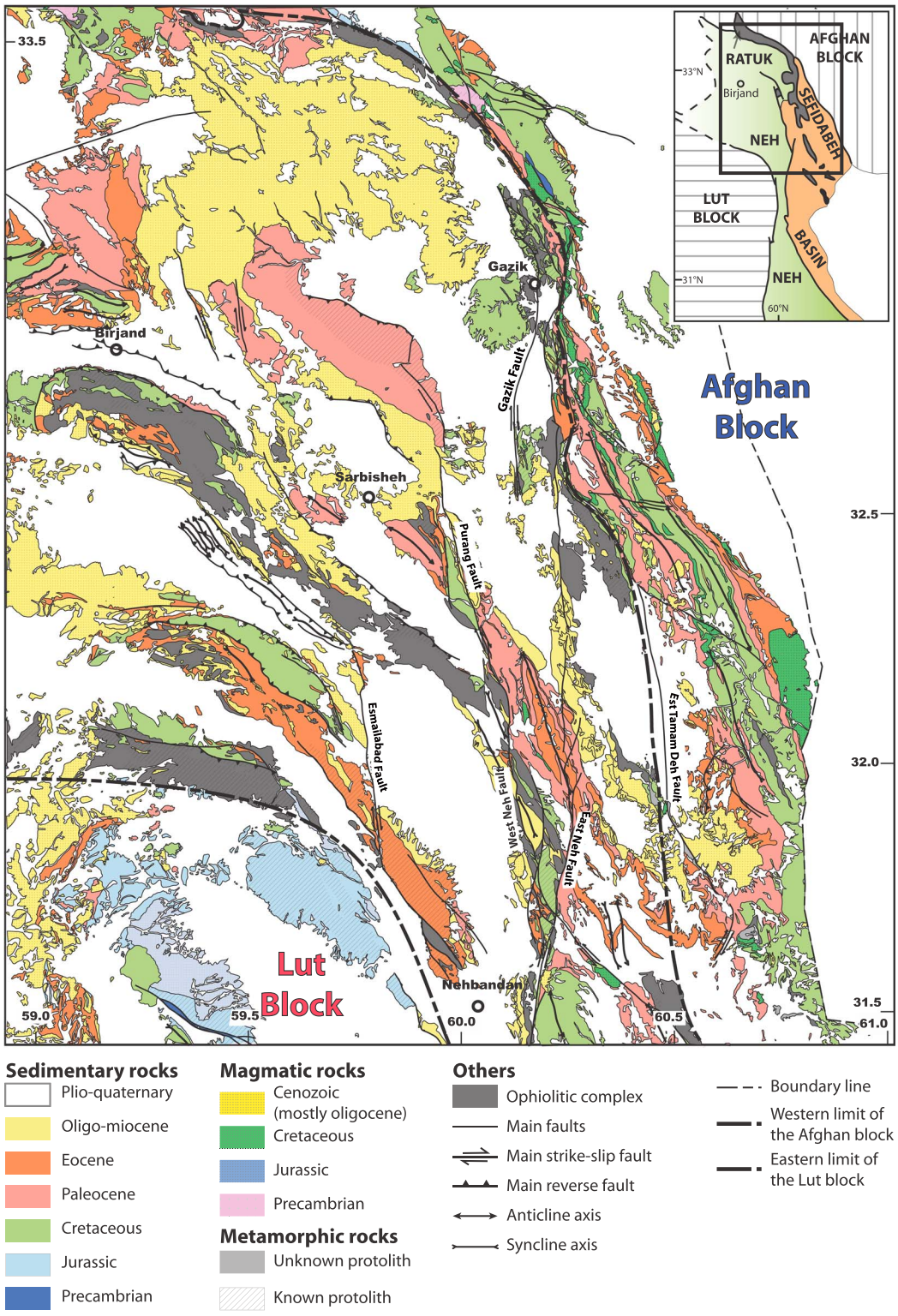


**Figure 2.** Geological and structural map of north Sistan domain.

Maastrichtian age. By contrast, the (4) Ratuk Complex is characterized by the presence of highly deformed and locally metamorphosed under HP-LT conditions, ophiolitic mélange, and metasediments (of similar Senonian to Maastrichtian age [*Babazadeh and De Wever*, 2004]). The (5) Sefidabeh basin, overlying both

the Ratuk and Neh complexes, consists of Senonian to Eocene turbiditic or molassic deposits and was interpreted as a fore-arc basin.

### 2.2. Tectonic Evolution of the Sistan Orogen

The Sistan belt displays a complex imbrication of thrust sheets, with rocks of various origins, variably deformed and metamorphosed. Peridotites, serpentinites, gabbros, and leucogabbros, dolerites, basalts, and radiolarites represent remnants of the lithosphere of the Sistan oceanic basin and its pelagic sedimentary cover [*Camp and Griffis*, 1982; *Moazzen et al*., 2006]. Biostratigraphic dating of radiolarites yielded early Aptian to late Albian ages [*Babazadeh and De Wever*, 2004]. Radiometric U-Pb dating of zircons from oceanic leucogabbros yielded an Albian ages between 107 ± 1 and 113 ± 1 Ma [*Zarrinkoub et al*., 2012], while K-Ar dating of amphiboles from oceanic gabbros yielded an Aptian age of 124 ± 11 Ma [*Delaloye and Desmons*, 1980], suggesting that the Sistan oceanic basin was widely opened by the mid-Cretaceous. Some authors [e.g., *Berberian and Berberian*, 1981] proposed that the Sistan basin opened as a back-arc basin above the Zagros subduction zone, which was already active at that time [*Agard et al*., 2011]. The Sistan ocean opened between two microcontinental blocks, the Lut block to the west and the Afghan block to the east, although its exact orientation is still somewhat speculative (Figures 1 and 2) [*Barrier and Vrielynck*, 2008; *Saccani et al*., 2010]. Rifting between the Lut and Afghan blocks may have started during the early (to middle) Cretaceous [*Delaloye and Desmons*, 1980; *Babazadeh and De Wever*, 2004], as for Sabzevar or Nain-Baft microoceans [*Moghadam et al*., 2009; *Agard et al*., 2011; *Shafaii Moghadam et al*., 2014]. A recent paleomagnetic study [*Mattei et al*., 2015] shows that Central Iran (defined by the Yadz, Tabas, and Lut blocks) suffered a homogeneous counterclockwise rotation of about 30° between the Late Jurassic to the Early Cretaceous supporting the idea of a coherent Central Iranian block at that time.

Radiometric Rb-Sr (on phengite and glaucophane from height samples), $^{40}Ar$-$^{39}Ar$ (on phengite coming from five samples) and U-Pb (on four samples zircons) dating on metamorphics rocks of the Sistan suture zone yielded an homogeneous Coniacian age between 85 and 87 Ma for the high-pressure parageneses [*Bröcker et al*., 2013]. The (probably est-vergent) subduction of the Sistan oceanic basin was thus already active in the Late Cretaceous. The deposition of a thick series of Late Cretaceous to Paleocene flysch accords with this geodynamic scenario (Figure 3).

Compared to the older, slightly metamorphosed Paleocene flysch deposits, Eocene deposits are unmetamorphosed, coarser-grained and more proximal (Figure 4) molasses-type sediments, indicating that collision probably started during the Eocene. Voluminous syncollisional to postcollisional Cenozoic magmatic rocks (volcanic to subvolcanic rocks, essentially) emplace over the Lut block and part of the Sistan suture zone (including ophiolitic units [*Camp and Griffis*, 1982]). These magmatic rocks are mildly deformed. Age constraints for these magmatic rocks span the mid-Eocene (46 Ma, on Ar-Ar dating) to the late Oligocene (25 Ma Ar-Ar whole rocks dating [*Pang et al*., 2013]). This magmatism has been interpreted as the result of the delamination of the lithospheric root during the collision [*Pang et al*., 2013].

Relatively minor shortening occurred during Miocene times (see below), while paleomagnetic data indicate that counterclockwise rotation (by ~35°) resumed in Central Iran since the middle to late Miocene [*Mattei et al*., 2012, 2015]. The Sistan suture zone is still tectonically active at present, as shown by several morphologic indicators (e.g., shifts of river waterways) and by instrumental seismicity and paleoseismicity studies of strike-slip faults (e.g., N-S right-lateral faults and their left-lateral conjugates associated with NW-SE reverse faults [*Berberian et al*., 2000; *Walker and Khatib*, 2006] (Figures 1 and 2).

### 2.3. Cenozoic Deformation Stages Recorded in Sistan Sedimentary Rocks

During the 1990s, 1:50,000 scale maps were merged into 1:250,000 scale maps. In order to have a synthetic view of all the northern part of the Sistan belt, we have grouped and homogenized together six of these 1:250,000 scale maps (Birjand, Dehsalm, Gazik, Qayen, Shahrakht, and Zabol) to obtain a structural map, showing the main faults and folds axes (Figure 2).

In the Sefidabeh basin three stages of deformation had been described [*Camp and Griffis*, 1982]. The (1) oldest stage is marked by the presence of approximately E-W trending axis folds. These folds are re-folded by smallest N-NW trending folds and dissected by conjugate strike-slip faults. (2) During the second stage, early Eocene sedimentary rocks were strongly deformed, whereas early Miocene subvolcanic rocks (23.3 ± 6.2 Ma by K-Ar on amphibole [*Tirrul et al*., 1980]) were much less deformed. Noteworthily, the top of the Eocene is an

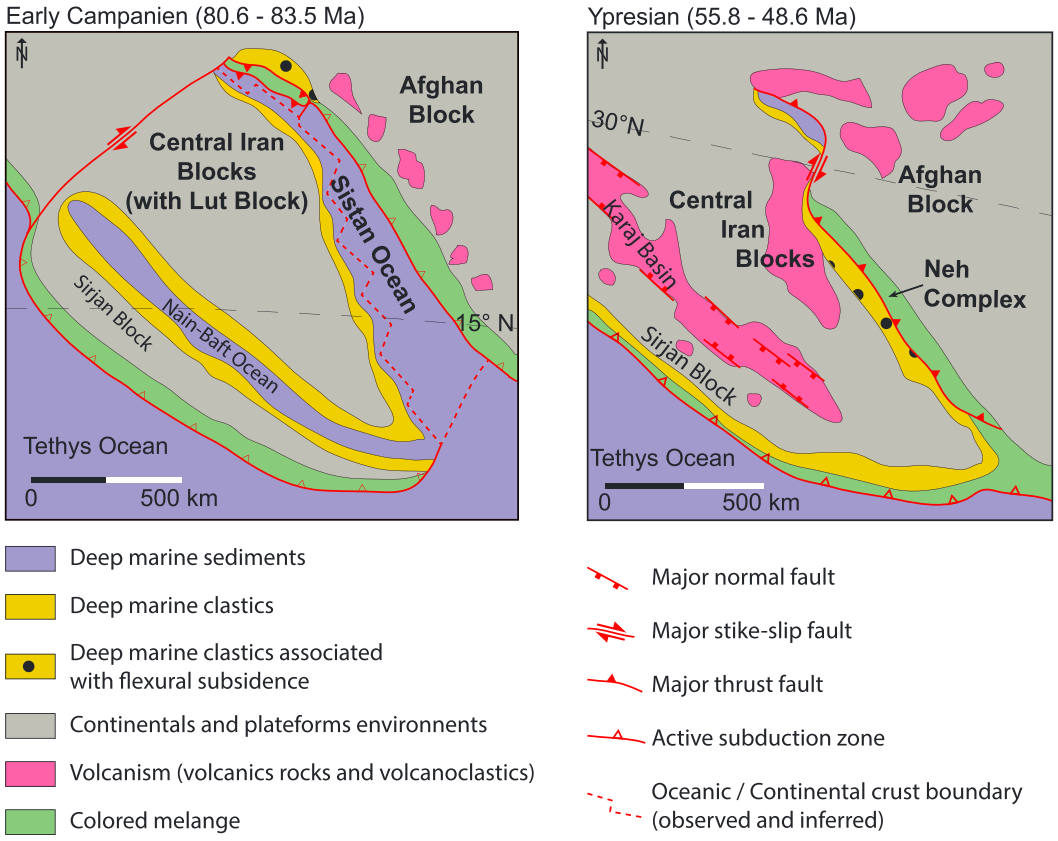


**Figure 3.** Tectonic Plates reconstruction for the Central Iran in early Campanian and Ypresian [modified from *Barrier and Vrielynck*, 2008].

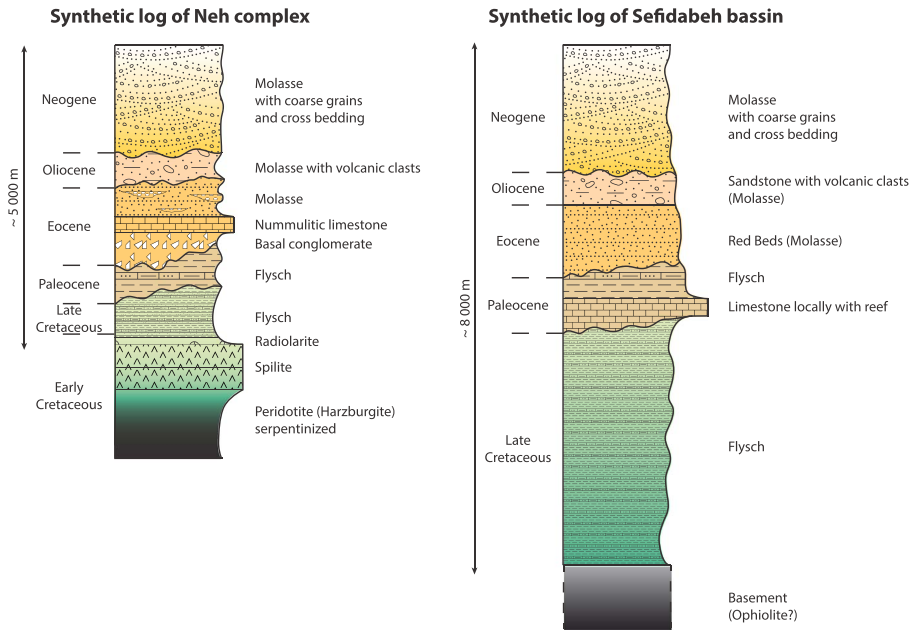


**Figure 4.** Synthetic logs of Neh complex and Sefidabeh basin.

important unconformity [*Freund*, 1970] and Oligocene deposits are also much less deformed than the Eocene ones [*Tirrul et al*., 1983]. These two first deformation stages likely took place during the Eocene. The youngest (3) stage of deformation, inferred to be Plio-Pleistocene age, is marked by gentle NNE-SSW trending folds affecting Oligocene deposits and by the reactivation of N-S trending right-lateral strike-slip faults (e.g., East and West Neh Faults and Zahedan Fault; Figures 1 and 2). This stage was attributed to the indentation of Central Iran by the Arabian plate [*Tirrul et al*., 1983].

Offsets of rock markers (e.g., Cretaceous ophiolites) and displacements of river valleys were used to estimate maximum displacements along the major right-lateral strike-slip faults: 13 to 20 km on the Zahedan fault, 50 to 65 km on the Est Neh fault, and around 10 km for the West Neh fault [*Walker*, 2006]. Most of this deformation is probably Plio-Quaternary, based on hills formed in recent alluviums [*Walker*, 2006]. Right-lateral strike-slip focal mechanisms are recorded along these active faults (e.g., 10 April 1998 and 20 June 1997 earthquakes [*Berberian et al*., 1999; *Walker*, 2006]), associated with ENE-WSW compressional events like the 24 November 1987 earthquake which nucleated south of Birjand [*Walker and Khatib*, 2006]. The present-day mean direction of compression ($\sigma_1$) is trending N10°E, i.e., parallel to the Arabia-Eurasia convergence measured by GPS (with ~25 mm/yr at the longitude 60°E [*Vernant et al*., 2004]).

The aim of this study is to fill the gap between preliminary studies dealing with the overall structure of the Sistan suture zone and recent investigations of active tectonics in this region.

## 3. Analysis of Fault Slip Data

### 3.1. Measurement Strategy and Determination of Stress Regime

More than 500 striated fault planes and numerous associated tectonic joints were examined and measured in 46 localities, mainly in the Sefidabeh basin and the Neh complex (Table 1 and Figure 5; all data are available in the supporting information). To the extent possible, several sites were selected in each stratigraphic unit (Figure 4) in both Neh and Sefidabeh units. We also selected outcrops far from the main regional faults (N-S right-lateral strike-slip fault), which may locally disturb the stress field [e.g., *Homberg et al*., 1997]. Based on the collection of fault slip data (kinematic, strike, dip, and striation for each fault, see the supporting information), the stress regime has been determined by using an inverse method [*Angelier et al*., 1982; *Angelier*, 1984, 1990].

The main aspect of this approach is to solve an inverse problem according to the Wallace-Bott's principle [*Wallace*, 1951; *Bott*, 1959]. This inverse problem is to determine the stress tensor knowing the direction and the sense of slip on a statistically relevant number of faults. It was first solved by *Carey and Brunier* [1974] and followed by various subsequent methodological developments and improvements [*Angelier*, 1975; *Armijo and Cisternas*, 1978; *Etchecopar et al*., 1981; *Angelier*, 1984; *Reches*, 1987]. Here we used Angelier's software in direct inversion mode (INVD). This method assumes that the striation occurs in the direction of the resolved shear stress (the tangential stress, i.e., the projection of the applied stress on the fault plane) on each fault plane, the fault plane being the preexisting fracture. Inversion computes a mean best fitting deviatoric stress tensor from a set of at least four striated faults by minimizing the angular deviation between a predicted slip vector (maximum shear) and the observed striation [*Carey*, 1979; *Angelier*, 1984; *Mercier et al*., 1991] This method assumes that rigid block displacements are independent. Inversion results include the orientation (azimuth and plunge) of the principal stress axes of a mean deviatoric stress tensor ($\sigma_1$, $\sigma_2$, and $\sigma_3$) as well as a stress ellipsoid shape parameter $\Phi$ ratio ($\Phi = (\sigma_2 - \sigma_3)/(\sigma_1 - \sigma_3) \leq 1$), where $\sigma_1$, $\sigma_2$, and $\sigma_3$ correspond to the compressional, intermediate, and extensional principal stress axes, respectively. With both orientation of stresses axes and $\Phi$ ratio, the stress regime can be determined: (a) when $\sigma_3$ is vertical, the stress regime is purely compressional (PC in Table 1) when $\Phi$ ratio is close to 0.5 (between 0.75 and 0.25, $\sigma_1 > \sigma_2 > \sigma_3$), radial compressional (RC in Table 1) when $\Phi$ ratio is close to 1 (between 0.75 and 1, $\sigma_1 \approx \sigma_2$), and transpressive (TP in Table 1) when $\Phi$ ratio is close to 0 (between 0.25 and 0, $\sigma_2 \approx \sigma_3$); (b) when $\sigma_1$ is vertical, the stress regime is purely extensional (PE in Table 1), when $\Phi$ ratio is close to 0.5, radial extensional when $\Phi$ ratio is close to 0, and transtensive (TT in Table 1) when $\Phi$ ratio is close to 1; (c) when $\sigma_2$ is vertical, the stress regime is purely strike slip (PSS in Table 1), when $\Phi$ ratio is close to 0.5, transtensive when $\Phi$ ratio is close to 1, and transpressive when $\Phi$ ratio is close to 0. Inversion results are generally considered reliable if 80% of the angular deviations between predicted slip vector and the observed striations are less than 22.5° in average.

**Table 1.** Trend and Dip of Principal Stress Axes Computed From Fault Slip Data[a]

| Site | nT | *n* | Formation | Age | $\sigma 1$ Strike, Dip (deg) | $\sigma_2$ Strike, Dip (deg) | $\sigma_3$ Strike, Dip (deg) | Φ | SR | RUP (%) | ANG (°) | Q | Latitude (°N) | Longitude (°E) |
|---|---|---|---|---|---|---|---|---|---|---|---|---|---|---|
| J6-1 | 6 | 6 | Conglomerate | Quaternary | 209, 12 | 119, 02 | 019, 77 | 0.68 | PC | 15 | 5 | B | 32°16′56.7″ | 59°43′16.5″ |
| Si-14b-16 | 20 | 20 | Conglomerate | Quaternary | 017, 00 | 287, 12 | 108, 78 | 0.68 | PC | 11 | 4 | A | 32°12′54.8″ | 60°03′56.2″ |
| Si-14b-18 | 15 | 15 | Conglomerate | Quaternary | 197, 06 | 106, 12 | 313, 77 | 0.52 | PC | 22 | 9 | A | 32°13′08.0″ | 60°03′56.1″ |
| Si-14b-29 | 8 | 8 | Conglomerate | Quaternary | 210, 06 | 119, 12 | 324, 76 | 0.44 | PC | 20 | 5 | A | 32°50′40.6″ | 59°19′47.5″ |
| Si-14b-31 | 9 | 9 | Conglomerate | Quaternary | 214, 02 | 123, 17 | 311, 73 | 0.12 | TP | 35 | 9 | B | 32°48′21.5″ | 59°25′04.4″ |
| Si-14b-6 | 6 | 6 | Conglomerate | Quaternary | 029, 02 | 298, 22 | 124, 68 | 0.11 | TP | 29 | 8 | B | 32°52′06.4″ | 59°16′28.1″ |
| Si-14b-7 | 7 | 7 | Conglomerate | Quaternary | 204, 02 | 294, 05 | 089, 85 | 0.64 | PC | 11 | 6 | B | 32°07′05.4″ | 60°01′44.2″ |
| Si-16-01 | 19 | 19 | Conglomerate | Quaternary | 204, 02 | 294, 11 | 101, 79 | 0.34 | PC | 19 | 7 | A | 32°35′53.7″ | 59°28′40.8″ |
| J8-13 | 6 | 6 | Conglomerate | Pliocene | 297, 13 | 171, 68 | 032, 17 | 0.94 | TP | 22 | 7 | B | 31°54′06.4″ | 59°38′47.9″ |
| J9-1 | 9 | 9 | Conglomerate | Pliocene | 154, 06 | 245, 12 | 037, 77 | 0.2 | TP | 13 | 11 | B | 31°38′01.9″ | 59°50′05.2″ |
| J5-8 | 23 | 23 | Conglomerate | Neogene | 231, 00 | 141, 05 | 326, 85 | 0.65 | PC | 19 | 9 | A | 32°15′30.5″ | 59°47′16.0″ |
| J6-2 | 6 | 6 | Conglomerate | Neogene | 073, 16 | 237, 74 | 341, 04 | 0.61 | PSS | 33 | 14 | C | 32°16′48.5″ | 59°43′20.1″ |
| J6-4 | 5 | 5 | Conglomerate | Neogene | 047, 04 | 139, 29 | 311, 61 | 0.06 | TP | 15 | 3 | A | 32°20′53.3″ | 59°38′24.6″ |
| Si-14b-20 | 24 | 24 | Conglomerate | Neogene | 052, 02 | 321, 14 | 150, 75 | 0.43 | PC | 32 | 12 | A | 32°41′49.8″ | 59°10′18.0″ |
| Si-14b-22 | 7 | 7 | Conglomerate | Neogene | 232, 07 | 324, 16 | 119, 72 | 0.61 | PC | 9 | 8 | B | 32°29′50.3″ | 59°27′32.9″ |
| Si-14b-28 | 4 | 4 | Conglomerate | Neogene | 069, 06 | 197, 81 | 338, 07 | 0.44 | PSS | 31 | 3 | B | 32°50′23.9″ | 59°19′40.3″ |
| Si-14b-5 | 9 | 9 | Conglomerate | Neogene | 228, 16 | 136, 06 | 028, 73 | 0.8 | RC | 22 | 7 | B | 32°52′25.0″ | 59°14′02.2″ |
| Si-14b-8 | 9 | 9 | Conglomerate | Neogene | 056, 19 | 148, 07 | 257, 70 | 0.08 | TP | 29 | 7 | B | 32°07′48.8″ | 60°02′37.7″ |
| Si-14b-1 | 5 | 5 | Sandstone | Oligo-Miocene | 087, 18 | 219, 65 | 351, 18 | 0.59 | PSS | 17 | 6 | B | 31°51′52.7″ | 60°10′55.5″ |
| Si-14b-2a | 15 | 15 | Sandstone | Oligo-miocene | 089, 07 | 179, 02 | 285, 83 | 0.58 | PC | 33 | 11 | B | 31°52′11.5″″ | 60°11′32.3″ |
| Si-14b-3a | 17 | 17 | Sandstone | Oligo-Miocene | 198, 15 | 106, 07 | 350, 74 | 0.03 | TP | 25 | 11 | A | 31°53′20.5″ | 60°11′57.1″ |
| Si-14b-3b | 7 | 7 | Sandstone | Oligo-Miocene | 259, 14 | 165, 16 | 028, 68 | 0.71 | PC | 30 | 6 | B | 31°53′20.5″ | 60°11′57.1″ |
| J4-4 | 5 | 5 | Conglomerate | Eocene | 250, 06 | 159, 06 | 023, 81 | 0.11 | TP | 16 | 4 | B | 32°21′15.6″ | 59°23′25.6″ |
| J4-7 | 9 | 9 | Carbonate | Eocene | 023, 02 | 291, 52 | 115, 38 | 0.14 | TP | 24 | 4 | A | 32°18′45.4″ | 59°22′56.9″ |
| J8-2 | 6 | 5 | Carbonate | Eocene | 247, 02 | 157, 02 | 027, 87 | 0.26 | PC | 33 | 10 | C | 32°04′13.9″ | 59°25′04.1″ |
| J11-13 | 8 | 8 | Carbonate | Eocene | 353, 06 | 102, 73 | 261, 16 | 0.37 | PSS | 43 | 18 | C | 32°43′14.6″ | 59°17′36.6″ |
| Si-15-3 | 8 | 8 | Carbonate | Eocene | 196, 14 | 286, 01 | 021, 75 | 0.58 | PC | 18 | 5 | A | 32°40′55.8″ | 59°21′11.0″ |
| J7-4a | 8 | 8 | Carbonate | Paleocene | 057, 51 | 257, 37 | 159, 10 | 0.5 | PE | 35 | 8 | B | 32°33′03.3″ | 60°22′34.9″ |
| J7-5 | 10 | 10 | Flysch | Paleocene | 067, 06 | 202, 82 | 336, 06 | 0.77 | TT | 32 | 10 | B | 32°33′23.2″ | 60°22′53.1″ |
| J7-6a | 14 | 14 | Carbonate | Paleocene | 095, 32 | 261, 57 | 001, 07 | 0.6 | PSS | 14 | 6 | A | 32°34′55.8″ | 60°22′05.1″ |
| J7-6b | 15 | 15 | Carbonate | Paleocene | 061, 00 | 331, 10 | 151, 80 | 0.36 | PC | 28 | 8 | A | 32°34′55.8″ | 60°22′05.1″ |
| J10-2a | 11 | 10 | Flysch | Paleocene | 308, 14 | 111, 76 | 217, 04 | 0.82 | TT | 32 | 6 | A | 32°45′39.4″ | 59°53′00.2″ |
| J10-2b | 14 | 14 | Flysch | Paleocene | 237, 13 | 337, 38 | 131, 49 | 0.23 | TP | 36 | 15 | B | 32°45′50.6″ | 59°53′24.6″ |
| Si-14-15 | 21 | 20 | Carbonate | Paleocene | 059, 21 | 245, 69 | 150, 02 | 0.9 | TT | 34 | 10 | A | 32°34′12.9″ | 60°23′20.0″ |
| Si-14-24 | 17 | 17 | Carbonate | Paleocene | 223, 04 | 115, 76 | 314, 13 | 0.54 | PSS | 52 | 19 | B | 32°20′40.1″ | 60°30′32.8″ |
| Si-14b-13 | 13 | 13 | Flysch | Paleocene | 084, 04 | 340, 74 | 175, 15 | 0.49 | PSS | 18 | 3 | A | 32°33′08.0″ | 60°23′10.1″ |
| Si-14b-14a | 14 | 14 | Carbonate | Paleocene | 263, 41 | 064, 48 | 165, 09 | 0.8 | TT | 21 | 10 | B | 32°33′01.1″ | 60°25′32.3″ |
| Si-14b-14b | 10 | 10 | Carbonate | Paleocene | 238, 01 | 147, 11 | 332, 79 | 0.18 | TP | 15 | 6 | A | 32°33′01.1″ | 60°25′32.3″ |
| Si-14b-19 | 15 | 15 | Carbonate | Paleocene | 088, 35 | 253, 54 | 353, 08 | 0.16 | TP | 39 | 7 | A | 32°18′03.9″ | 60°04′11.3″ |
| Si-14b-23 | 4 | 4 | Carbonate | Paleocene | 237, 40 | 055, 50 | 146, 01 | 0.52 | PSS | 32 | 6 | B | 32°17448.3″ | 60°29′43.5″ |
| Si-14b-25 | 14 | 14 | Carbonate | Paleocene | 244, 12 | 335, 02 | 076, 78 | 0.11 | TP | 28 | 14 | B | 32°19′44.6″ | 60°34′50.2″ |
| Si-15-1 | 9 | 9 | Flysch | Paleocene | 206, 07 | 299, 24 | 101, 65 | 0.52 | PC | 36 | 13 | B | 33°04′28.5″ | 59°40′16.3″ |
| Si-15-2 | 12 | 12 | Carbonate | Paleocene | 218, 03 | 127, 05 | 335, 84 | 0.19 | TP | 41 | 13 | B | 32°02′38.4″ | 59°34′05.2″ |
| J7-3-2 | 13 | 13 | Flysch | Upper Cretaceous | 018, 23 | 202, 67 | 109, 01 | 0.51 | PSS | 30 | 11 | B | 32°33′00.1″ | 60°22′34.4″ |
| J11-10 | 7 | 7 | Sandstone | Upper Cretaceous | 244, 08 | 083, 82 | 334, 03 | 0.09 | TP | 31 | 9 | B | 32°44′50.3″ | 59°18′10.9″ |
| J11-8 | 6 | 6 | Flysch | Upper Cretaceous | 225, 14 | 009, 73 | 133, 10 | 0.5 | PSS | 51 | 13 | C | 32°45′25.3″ | 59°22′42.9″ |
| Si-14b-26 | 16 | 16 | Sandstone | Upper Cretaceous | 271, 20 | 052, 65 | 176, 14 | 0.38 | PSS | 30 | 9 | A | 32°22′31.6″ | 60°37′04.3″ |

[a]nT is the number of fault data measured. *n* is the number of fault data used for stress tensor calculation. $\sigma_1$, $\sigma_2$, and $\sigma_3$ correspond to the maximum, intermediate, and minimum principal stress axes, respectively. Φ is the ratio $(\sigma_2 - \sigma_3)/(\sigma_1 - \sigma_3)$. SR is the stress regime with six types: (1) PC: pure compressional, (2) PE: pure extensional, (3) PSS: pure stike-slip, (4) RC: radial compressional, (5) TT: transtensive, and (6) TP: transpressive. RUP in per cent is a quality estimator parameter ("ratio upsilon") resulting from the INVD algorithm defined in *Angelier* [1990]. In average, if RUP ≤ 50, stress tensor is good; if 50 < RUP ≤ 75, stress tensor is acceptable; and if RUP > 75, stress tensor is not reliable [*Angelier*, 1990]. ANG is the average angle, in degrees, between slip vectors of all faults used and computed shear stress. Q is the quality ranking of the stress tensor calculated as in *Delvaux et al.* [1997]: (*n**(*n*/nT)/ANG). For Q > 1.5 stress tensor quality is good (A), for 1.5 ≥ Q > 0.5 stress tensor quality is medium (B), for 0.5 ≥ Q > 0.3 stress tensor quality is poor (C), and for Q ≤ 0.3 stress tensor is not reliable (D) [*Delvaux et al.*, 1997].

For a few outcrops (J6-4, Si-14b-1, Si-14b-7, and Si-14b-16), the inversion results are poorly constrained because the geometry and kinematics of the faults are too similar (open arrows in Figures 6 to 9) [*Angelier*, 1990].

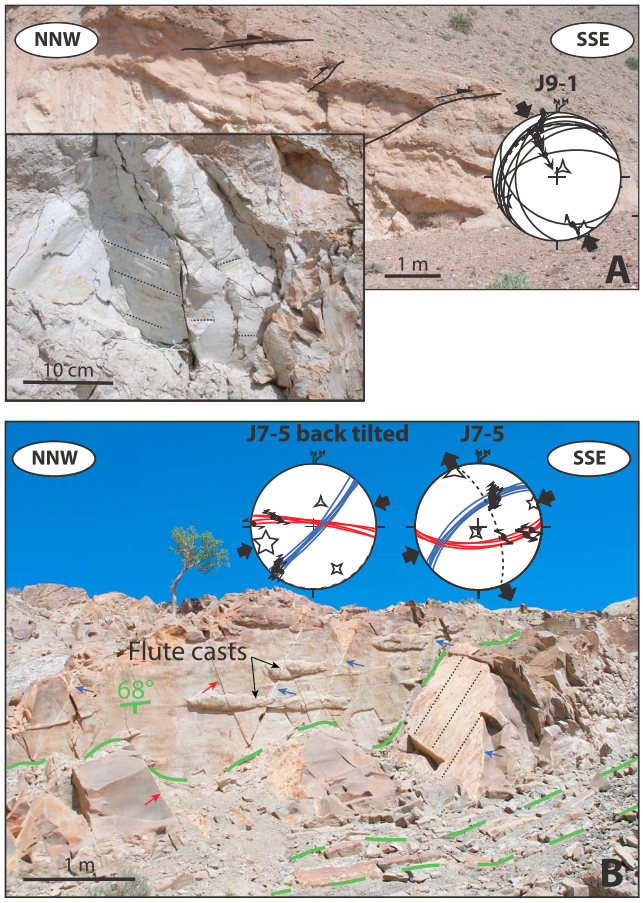


**Figure 5.** Examples of studied outcrops. (a) Plio-quaternary conglomerate with recent faulting. (b) Paleocene sandstone folded (bedding in green dashed lines: N158-68E) with tilted faults.

When fault slip data are too complex to be interpreted by a single stress tensor because of a mechanical incompatibility, generally due to superimposed tectonic events, we separated homogeneous fault subsets based on both fault orientation and striation. An inversion was performed for each subset and labeled with a or b suffix (e.g., sites Si-14b-3a and b and Si-14b-14a and b) if reliable.

Moreover, in folded areas, it is necessary to determine the timing of faulting relative to folding and subsequent bed tilting [*Yamaji et al.*, 2005]. Faults may have formed before, during, or after folding. Following *Anderson* [1942], we assume that away from major fault zones, one of the three principal stress axes of a tensor is generally vertical [*Bergerat*, 1987; *Fabbri*, 2000; *Fournier et al.*, 2008]. Whenever a fault set forms before folding and is secondarily tilted with the bedding, the tensor calculated on this set does not display a vertical axis, yet one of the stress axes is found perpendicular to bedding (the two others lying within the bedding plane). In such a case, the fault system can be interpreted after back-tilting to its initial position. One example of back-tilting is presented in Figure 5. In site J9-1 (Figure 5a), where conjugate reverse faults gently crosscut dipping strata of Plio-Quaternary conglomerates (10° dip), back-tilting is not necessary, contrary to site J7-5 (Figure 5b), where conjugate strike-slip faults crosscut steeply dipping strata of Paleocene sandstones (~70° dip) with flute casts, making back-tilting necessary. In this particular example, back-tilting does not change so much the direction of $\sigma_1$, but this is not the case in general (e.g., J10-2b and J11-10).

The chronology between the various stress tensors is based on the age of the faulted deposits. Results are presented from the youngest to the oldest deposits.

### 3.2. Fault Slip Analysis Across the Successive Deposits

Fault data were collected in the following units (Table 1 and Figure 6):

1. Eighteen outcrops in Plio-Quaternary conglomeratic rocks. They show dominantly reverse and strike-slip faults and the corresponding stress regime, with mainly pure compression ($n = 9$) or transpression ($n = 6$), even if two pure strike-slip regimes and one with radial compression were also found (Table 1). Based on the direction of the maximum horizontal stress ($\sigma_1$), two subsets were separated: one with $\sigma_1$ around N25°E (blue arrows in Figure 6) and one with $\sigma_1$ around N60°E (red arrows). There are also two outcrops (J8-13 and J9-1) showing a totally different direction of $\sigma_1$ (black arrows in Figure 6), which are discussed in section 4.2.
2. Only few outcrops in Oligo-Miocene deposits provided reliable stress tensors (see Figure 2). Faults observed are mainly reverse or strike slip in one locality. The direction of $\sigma_1$ is around 25°N (blue arrow in Figure 6) or around 90°N (green arrow).

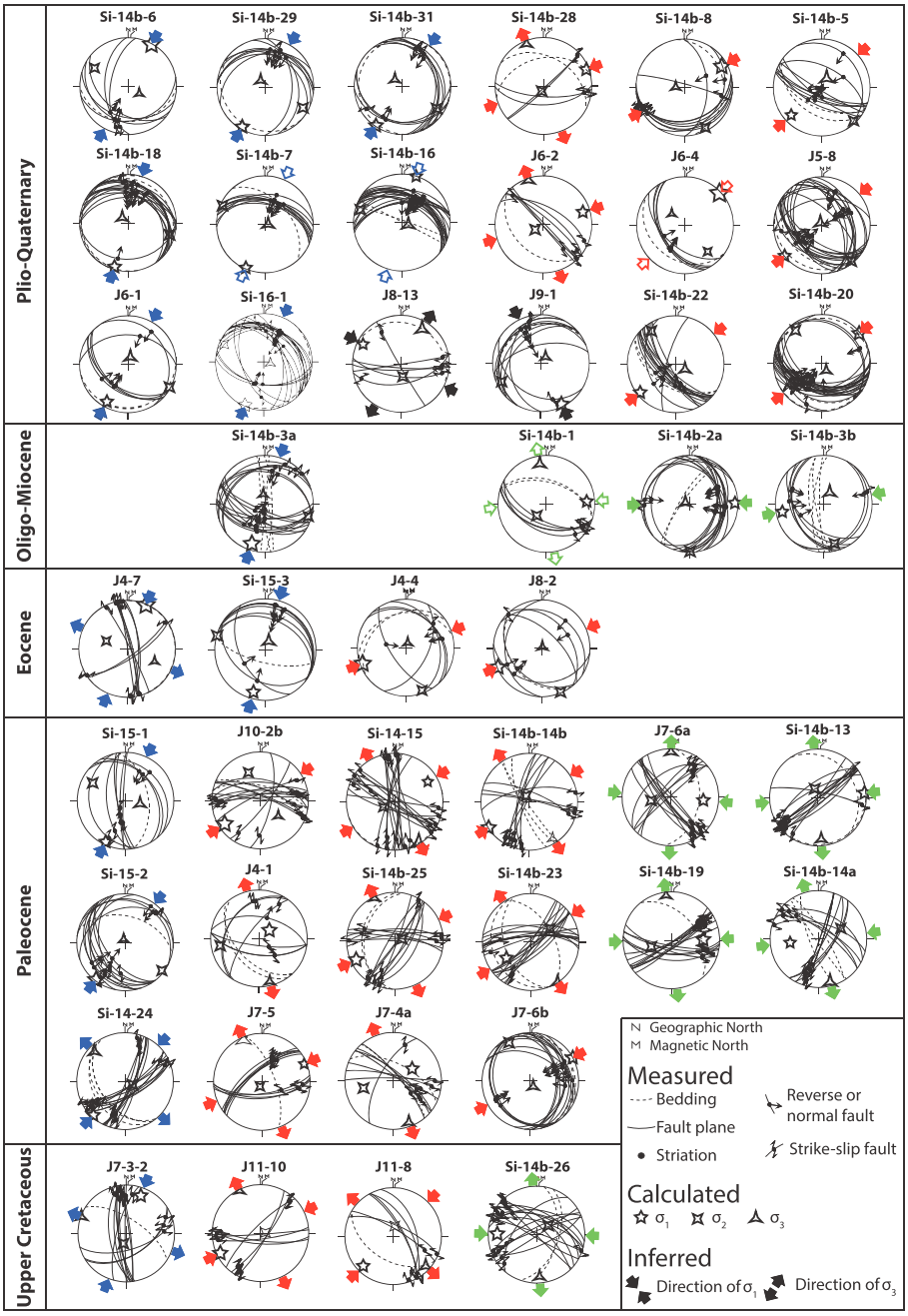


**Figure 6.** Synthesis of late Cenozoic brittle deformation in the northern part of the Sistan belt. Three successive directions of compression ($\sigma_1$) are identified: (1) a N90°E trending compression during the middle-late Miocene (green arrows), (2) a N60°E trending compression during the late Pliocene (red arrows), and (3) a N25°E trending compression during the Plio-Quaternary (blue arrows). Stereonets show fault slip data in equal-area lower hemisphere projection, and arrows indicate the trend of the horizontal principal stresses computed (solid arrows) or inferred (open arrows). Stars in stereonets correspond to the principal stress axes: $\sigma_1$ (five branches), $\sigma_2$ (four branches), and $\sigma_3$ (three branches). The dashed line is for the bedding plane.

3. Four outcrops of Eocene age (three in carbonates and one in conglomerates). The stress regime is purely compressional or transpressive. The $\sigma_1$ strikes either around 25°N or 60°N.
4. Sixteen outcrops in Paleocene in carbonate and flysch. These corresponding stress regimes are transpressive, transtensive, purely strike slip, and purely compressional, with a direction of $\sigma_1$ compatible with one of the three directions previously defined (see the color of the arrows).

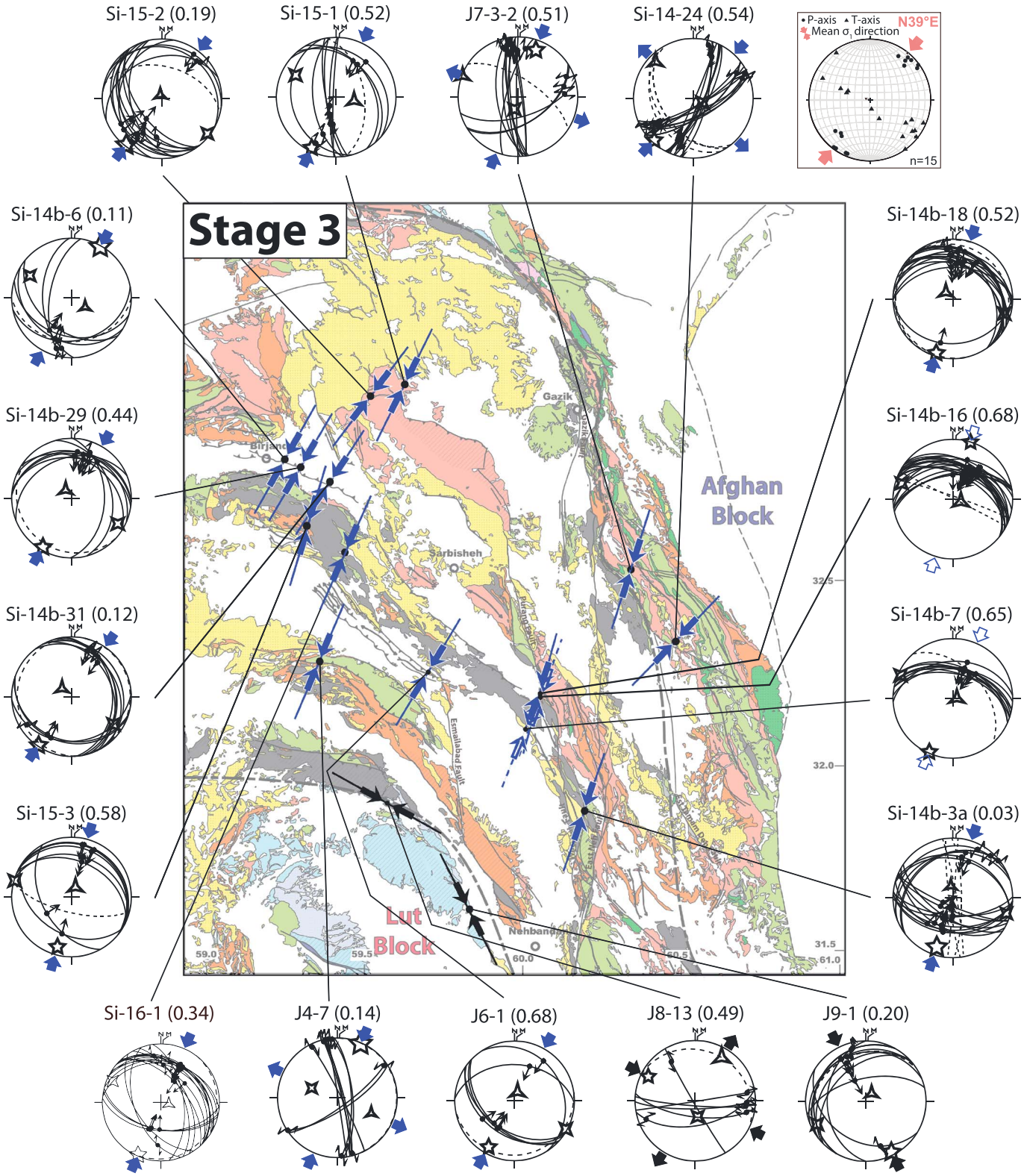


**Figure 7.** N25°E compression (on average) recorded in the upper Cretaceous to Plio-Quaternary formations of the Neh complex and Sefidabeh basin. Φ ratio is indicated near the site name (in bracket). The top right insert shows equal-area projection of compression *P* and tension *T* axes of fifteen Harvard centroid moment tensor of earthquakes shallower than 30 km which occurred between 1976 and 2015 in North Sistan. All the focal mechanisms are of the compressional or strike-slip type. All *P* axes are nearly horizontal and trend between N23°E and N56°E with a mean trend of N39°E [*Dziewonsky et al.*, 1981; *Marrett and Allmendinger*, 1990].

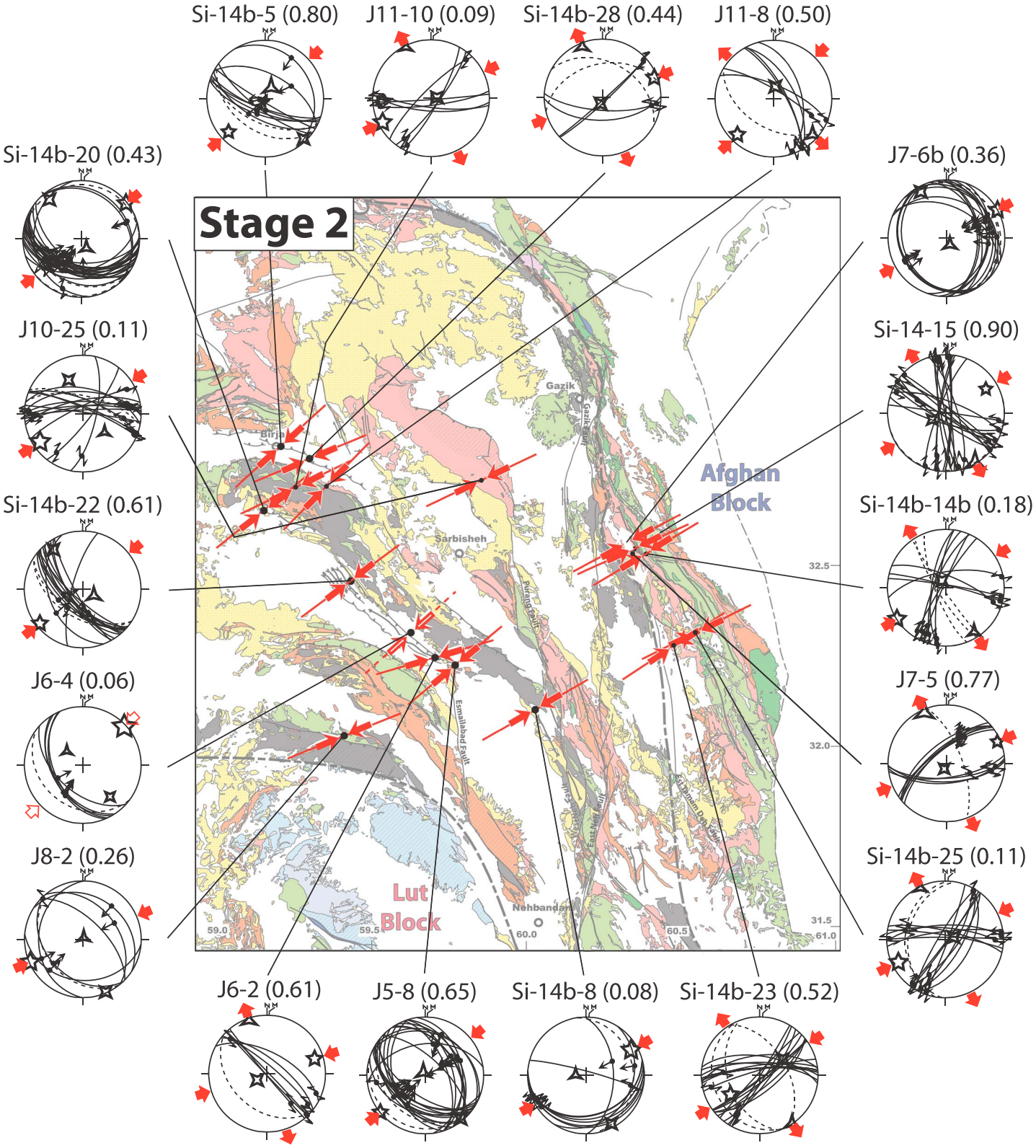


**Figure 8.** N60°E compression (on average) recorded in the Upper Cretaceous to Plio-Quaternary formations of the Neh complex and Sefidabeh basin. Φ ratio is indicated near the site name (in bracket).

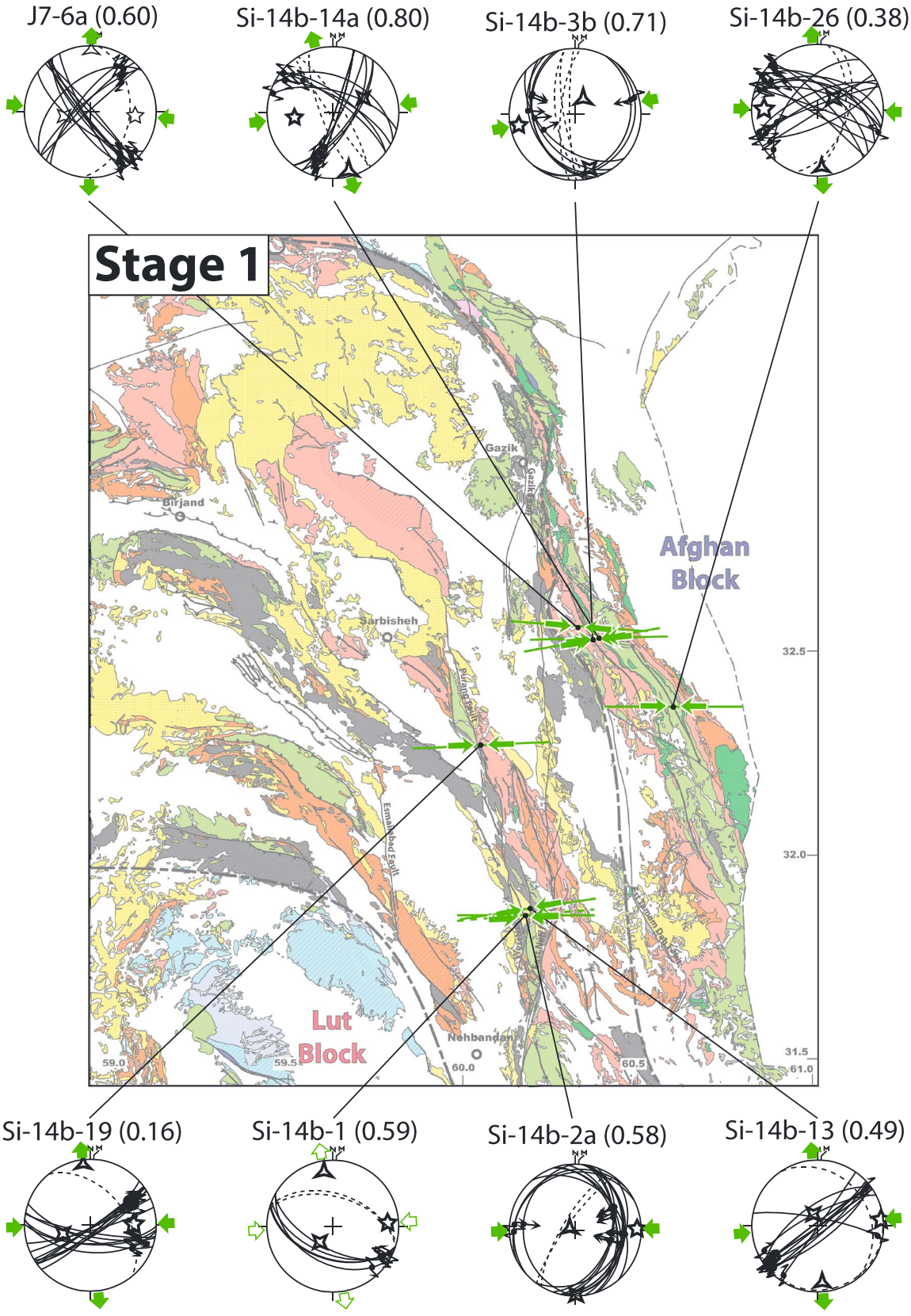


**Figure 9.** N90°E compression (on average) recorded in the Upper Cretaceous to Miocene formations of the Neh complex and Sefidabeh basin. Φ ratio is indicated near the site name (in bracket).

5. Four outcrops of Cretaceous in sandstone and flysch. Faults observed are mainly strike slip, and stress regimes are purely strike slip or transpressive. The direction of $\sigma_1$ is always compatible with one direction previously defined (see the color of the arrows).

## 4. Interpretation and Discussion

### 4.1. Data Consistency and Stress Regime Through Time in the Sistan Region

After inversion (and back-tilting of the stratification, whenever required), all data sets provide one horizontal $\sigma_1$ axis and one vertical principal stress (Figure 6), indicating that the stress fields is Andersonian [*Anderson*, 1942]. All data sets, however, do not pertain to a unique stress field. Based on the direction of the maximum principal stress $\sigma_1$ and on the age of faulted formations, three successive episodes of deformation can be recognized:

1. The most recent one is characterized by two systems of reverse and strike-slip faults consistently indicating an average a 26°N ± 8° (standard deviation) direction of compression ($\sigma_1$). It was found in 15 outcrops all around the studied area and affects Cretaceous to Plio-Quaternary strata (Figures 6 and 7 and Table 1). Several arguments help to constrain the timing of this deformation between the late Pliocene and Present: (a) This stage of deformation was recognized in outcrops Si-14b-16 and Si-14b-18, which are located in the conglomeratic core of the late Pliocene to Pleistocene Chahkuh syncline (according to Porang geological map [*Nabavi and Shahrabi*, 1981]), and in outcrop Si-14b-7 located in the conglomeratic core of the similarly late Pliocene to Pleistocene Shurak syncline. Measurements in older sandstone strata from the rim of the latter syncline (outcrop Si-14b-8) yielded a different stress orientation (Figure 8). (b) In the Birjand anticline, the direction of compression ($\sigma_1$) around ~25°N was observed only in late the upper Pliocene conglomeratic deposits (age deduced from radiometric dating on basalts interbedded with these sedimentary rocks, according to Gazik geological map [*Fauvelet and Eftekhar-Nezhad*, 1990]), in contrast with the early Pliocene sandy deposits with more fine grains (according to Birjand geological map [*Eftekhar-Nezhad and Vahdati Danesmand*, 1991]). (c) This compression direction is mechanically compatible with the one deduced for the major active faults reported in the area (N-S dextral strike-slip faults and NNW-SSE reverse faults (Figure 2) [*Berberian et al*., 2000; *Walker and Khatib*, 2006]). (d) This compression direction is consistent with the mean trend of compressional *P* axes of earthquake focal mechanisms in north Sistan. This is shown by the equal-area projection of compression *P* and tension *T* axes for all 15 earthquakes shallower than 30 km, which occurred between 1976 and 2015 (Figure 7, top right insert) (source: Harvard centroid moment tensor catalog [*Dziewonski et al*., 1981]). (e) The direction of compression N25°E is close to the direction of GPS motions relative to stable Eurasia around N10°E (Figure 1). (f) Finally, a similar orientation was found for the youngest microtectonic episode in Central Iran [e.g.; *Navabpour et al*., 2007; *Shabanian et al*., 2010; *Karagaranbafghi et al*., 2012]. We discuss how this late Pliocene to present-day deformation may be related to the Arabia-Eurasia convergence in section 4.2 below.
2. The second stage of deformation is characterized by two systems of reverse and strike-slip faults consistently indicating in average a 59°N ± 8° (standard deviation) compression. It is observed in 20 outcrops located over the whole area, within Cretaceous to Pliocene strata (Figures 6 and 8 and Table 1). The youngest rocks affected by this deformation (outcrops J5-8, J6-2, Si-14b-05, and Si-14b-8) are of late Pliocene age [*Eftekhar-Nezhad and Vahdati Danesmand*, 1991; *Nabavi and Shahrabi*, 1981], advocating for a syn to post-late Pliocene deformation, slightly older than the one above.
3. The third deformation stage is characterized by almost E-W compression (~87°N ± 5°; Figures 6 and 9 and Table 1). It was documented in eight outcrops by two compatible systems of reverse and strike-slip faults, mainly in the east and south-east part of the studied area. It affects strata of Cretaceous to Oligo-Miocene age, suggesting that this deformation dates back to the late Miocene. The Oligo-Miocene series consists of brown to red continental conglomerates.

Two outcrops of Plio-Quaternary sediments on the edge of the Lut block (J8-13 and J9-1) show quite different orientations for $\sigma_1$ (black arrows on Figures 6 and 7). This dissimilarity could hypothetically result from local rotations due to the activity of the major fault located at the boundary between the Lut block and the Neh complex.

It is also worth mentioning that we could not evidence brittle deformation older than the Neogene in the field. Although previous tectonic studies documented discrete Paleogene stages of deformation, at least two, in the Sefidabeh Basin [*Freund*, 1970; *Tirrul et al*., 1980; *Camp and Griffis*, 1982; *Tirrul et al*., 1983], associated brittle structures (accommodating these deformations at small scale) have either not been observed or obliterated by the younger deformation described above.

To summarize, three distinct late Cenozoic compressional stages were recognized throughout the region: (1) an ~E-W compression, probably late Miocene; (2) a late Pliocene ENE-WSW compression; and (3) an ubiquitous late Pliocene to present-day deformation stage striking almost NNE-SSW. This indicates that within the last ~10–5 Myr, the main stress direction rotated about 60° counterclockwise in Sistan.

### 4.2. Paleostress Regime Across Iran During the Late Cenozoic

Paleostress data (from fault analysis or calcite twins) as well as present-day stress field estimates (from earthquake focal mechanisms) are available for most of Iran due to a wealth of recent publications, particularly in the Zagros region [*Authemayou et al*., 2005, 2006; *Lacombe et al*., 2006; *Aubourg et al*., 2010; *Lacombe et al*., 2011; *Navabpour and Barrier*, 2012; *Karagianni et al*., 2015] and along the Doruneh fault [e.g., *Farbod et al*., 2011; *Javadi et al*., 2013, 2015]. This information is compiled in Figure 10. Most of the inferred orientations match at least one of the three stages reported in section 4.1 (Figures 6–9).

Figure 10a shows that the orientation of the maximum principal stress ($\sigma_1$) determined for the late Pliocene to Present is relatively homogenous across Iran, irrespective of data type, suggesting far field stress control [*Zoback and Zoback*, 1989] by the Arabia-Eurasia convergence. This is true for the Zagros (with a clear obliquity between $\sigma_1$ and the main tectonic structures), Central Iran, and also for the Sistan belt, and even for the Makran region where the last piece of Neotethys is presently subducting. Only in a few cases does the orientation of the main stress differ significantly, notably in Lorestan and in the Alborz, where compression is locally perpendicular to the main (E-W) tectonic structures and in the eastern part of the dextral strike-slip Doruneh fault where compression is more ENE-WSW, probably due to a complex geometry implying a small rigid block (Yazd Block [*Farbod et al*., 2011; *Nozaem et al*., 2013; *Calzolari et al*., 2016a, 2016b]).

The orientation of $\sigma_1$ determined for the Miocene (in fewer places) is more variable in space (Figure 10b), with a marked contrast between the Zagros, on the one hand, and Iran's hinterland (Central Iran, Sistan, and Kopet Dagh), on the other hand. This situation also contrasts with the second stage of deformation reported in section 4.1, likewise of late Pliocene age, for which compression is almost parallel to the one inferred for the Zagros (Figure 10c).

Except for east Alborz area where the stress evolution through time shows a clockwise rotation [*Javidfakhr et al*., 2011a, 2011b], most areas thus evidence a counterclockwise rotation of compression with time, from the Miocene to Present (Figure 10). The amount of rotation is higher in central and north-east of Iran than in the west and south regions (Makran and Zagros) where, in some places, the direction of compression remains unchanged during the Neogene [*Authemayou et al*., 2006]. The amount of rotation is in fact probably underestimated for Central Iran and Sistan because paleomagnetic data indicate an ~35° counterclockwise block rotation after the middle-late Miocene (with 20° achieved since 10 Ma [*Mattei et al*., 2012, 2015]). This rotation is seemingly confined to these areas and does not extend to the Zagros, so that (i) compression may have been at right angle in Central Iran and Sistan with respect to Zagros during the Miocene and (ii) compression directions may have turned there counterclockwise by up to 110–120°.

Reorientation of compression in the Zagros was interpreted as recording local rotations of small crustal blocks along strike-slip faults (e.g., in the Fars domain [*Lacombe et al*., 2006]) or the progressive reorientation of Arabia-Eurasia convergence during the Cenozoic [*McQuarrie*, 2003; *Navabpour et al*., 2007]. The E-W direction of shortening in Central Iran during the Miocene can hardly be due to the Arabia-Eurasia convergence, especially if the 35° counterclockwise rotation is taken into account.

### 4.3. Regional-Scale Tectonic and Kinematic Implications

The relatively homogeneous present-day state of stress field across much of Iran (with $\sigma_1$ trending ~25°N; Figure 10a) suggests that stresses from the Arabia-Eurasia collision zone are transferred throughout the Iranian crust/lithosphere. It is interesting to note that a similar stress orientation presently prevails in

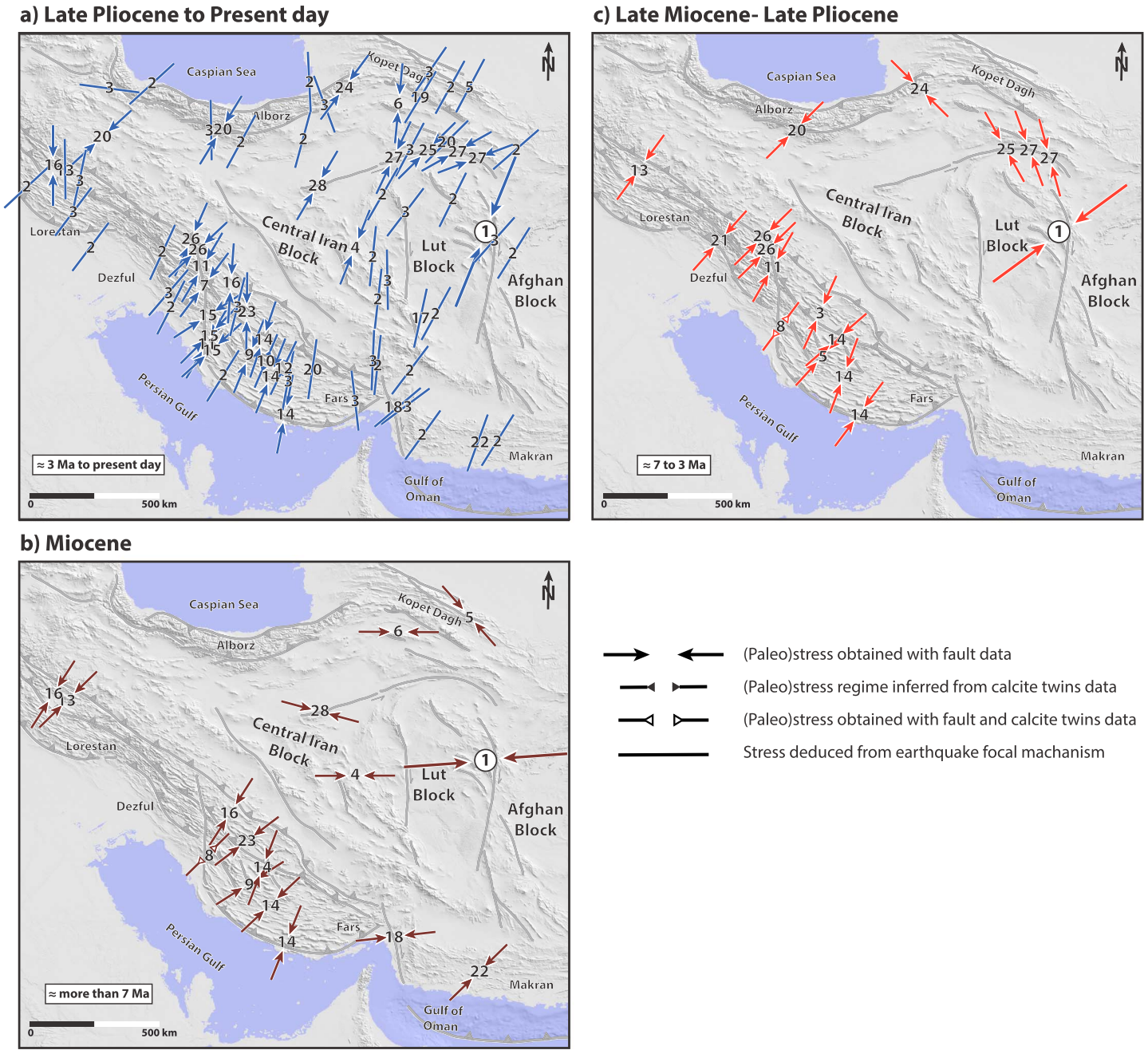


**Figure 10.** Topographic map of Iran (SRTM 30) with orientation of the principal stress (azimuth of $\sigma_1$) for (a) present day, (b) Miocene, and (c) intermediate period (late Miocene to late Pliocene). The type of arrow depends on methodology used to obtained stress: faults slip data, calcite twins, or earthquake focal mechanism. [1: this study; 2: *Zarifi et al.*, 2014; 3: *Karagianni et al.*, 2015; 4: *Kargaranbafghi et al.*, 2011; 5: *Shabanian et al.*, 2010; 6: *Yazdi et al.*, 2012; 7: *Authemayou et al.*, 2005; 8: *Aubourg et al.*, 2010; 9: *Lacombe et al.*, 2006; 10: *Lacombe et al.*, 2007; 11: *Authemayou et al.*, 2006; 12: *Walpersdorf et al.*, 2006; 13: *Navabpour et al.*, 2007; 14: *Lacombe et al.*, 2011; 15: *Mobasher and Babaie*, 2008; 16: *Navabpour and Barrier*, 2012; 17: *Fattahpour and Moosavi*, 2010; 18: *Regard et al.*, 2004; 19: *Zamani et al.*, 2008; 20: *Zanchi et al.*, 2006; 21: *Ahmadhadi et al.*, 2008; 22: *Dolati and Burg*, 2013; 23: *Navabpour et al.*, 2008; 24: *Javidfakhr et al.*, 2011a, 2011b; 25: *Farbod et al.*, 2011; 26: *Malekzade et al.*, 2016; 27: *Javadi et al.*, 2013; 28: *Javadi et al.*, 2015].

India, Pakistan, and Nepal (i.e., 023°N [*Gowd and Srirama Rao*, 1992; *Karagianni et al.*, 2015]), questioning whether this is coincidental or results from larger-scale dynamics driven by Neo-Tethyan closure. By contrast, present-day compression in Turkmenistan strikes NNW-SSE [*Karagianni et al.*, 2015], so that the influence of the Arabia-Eurasia convergence (at least to the NE) seems to die out ~1000 km away from the suture zone.

During the (early) Miocene "soft collision" stage (i.e., pre-15–10 Ma [*Ballato et al*., 2011]), the orientation of compression in the Zagros striked 45°N on average, which is also close to the only paleostress determination for Makran for the period [*Shabanian et al*., 2010; *Dolati and Burg*, 2013]. This orientation is at odds with the Sistan (and Central Iran in general) Miocene E-W (Figure 10b) to NNW-SSE compression (considering the 35° counterclockwise rotation of Central Iran and Sistan after the middle-late Miocene [*Mattei et al*., 2012, 2015]) and suggests that Sistan and Zagros were mechanically decoupled during the (early) Miocene. Whether this E-W to NNW-SSE compression corresponds to the one prevailing at the end of Sistan collision, which initiated during the Eocene (see section 2), is a matter of speculation. This direction (~125°N) matches the direction of shortening inferred for the Kopet Dagh (Figure 10b) [*Shabanian et al*., 2010], but paleostress data are lacking in the Alborz. Another potential stress source could be in the SE of Sistan, in the Chaman transform zone, where deformation is marked by N-S compression during the late Oligocene or early Miocene [*Lawrence et al*., 1981]. Additional paleostress determinations and more precise age data, especially in Central Iran, would be needed to conclude on this.

Progressive reorientation, during the late Miocene to Present, of the stress regime in eastern Iran toward stress directions prevailing in the Zagros (and/or Makran) could result from the intensification of Zagros collision from late Miocene times onward (~10 Ma to present, "hard collision" [*Agard et al*., 2011; *Ballato et al*., 2011; *Mouthereau et al*., 2012]). Considering this, Figure 10 might even suggest, despite the small number of studies, that from the Miocene to late Pliocene, regions close enough to the Zagros (i.e., within ~750 km: central Alborz, Central Iran, and Sistan) were stressed by the Zagros collision, and that this stress later spread, between late Pliocene to Quaternary, to more remote areas (e.g., Kopet Dagh).

This scenario is also in good agreement with most of the kinematic evolution of the main Central Iran faults (Figure 1): (a) activation of the N-S right-lateral strike-slip fault of the eastern Iran since the last 5 Ma and associated counterclockwise rotation of the Central Iranian Blocks [*Walker and Jackson*, 2004; *Walker and Khatib*, 2006; *Nozaem et al*., 2013]; (b) more recent (Plio-Quaternary) kinematic shift between left-lateral to right-lateral strike-slip fault in the northern border of Central Iran, especially along the Doruneh fault [*Farbod et al*., 2011; *Calzolari et al*., 2016a, 2016b].

## 5. Conclusion

The inversion of fault kinematic data reveals drastic temporal changes in the stress regime of eastern Iran during the late Cenozoic, with a marked counterclockwise rotation of at least 60° over the last 10–5 Myr of the main direction of shortening ($\sigma_1$), from 90°N during the middle-late Miocene to 60°N during the late Pliocene and 25°N during the Plio-Quaternary.

Our compilation of paleostress data indicates that the Plio-Quaternary direction of compression is relatively homogeneous throughout Iran and coincides with present-day Arabia-Eurasia convergence, advocating for effective stress transfer from the actively deforming Zagros collision across all Iranian crust/lithosphere. On the other hand, Miocene compression evidences a conspicuous contrast between the Zagros orogen and the Iranian hinterland (e.g., Sistan, Central Iran, and Kopet Dagh), where reconstructed directions of shortening strike consistently E-W. This E-W Miocene compression is not well understood yet and could tentatively represent shortening associated with the end of Sistan collision or the imprint of active deformation occurring further to the east, e.g., the activation of the Chaman transform zone to the SE (Pakistan). The intermediate orientation of the late Pliocene compression (i.e., 60°N) could correspond to the progressive (or transient) reorientation of the stress regime as the Sistan domain gets mechanically coupled to the Zagros during hard collision.

**Acknowledgments**
The authors would like to thank Associate Editor Claudio Faccenna and Editor Paola Vannucchi for accurate and constructive reviews of the manuscript at different stages. The reviewers, Christine Authemayou, Frederico Rosseti, and Andrea Zanchi, are acknowledged for their comments and suggestions, which significantly improved the manuscript. We feel indebted to the Geological Survey of Iran, and especially to Koreie; to the geologists (H.R. Karimi, R. Kohansal); and all the staff (drivers, cookers, and chief of camp) for their kindness, constant support, and for enabling us to visit the region since 2014. We also would like to warmly thank M. Zarrinkoub for his great help during field work. P. Agard acknowledges the support from the International Lithosphere Programme and from Institut Universitaire de France. This study also comes as a side project to the ANR ONLAP project funded by the Agence Nationale de la Recherche (ANR-10-BLAN-0615). The data used are listed in the references, figures, Table 1, and supporting information. All data provided in this study may be obtained by contacting the corresponding author by e-mail at michael.jentzer@upmc.fr or by letter at Michael Jentzer, site Jussieu, boîte courrier 34, 4 place Jussieu 75005, Paris.

## References

Agard, P., J. Omrani, L. Jolivet, H. Whitechurch, B. Vrielynck, W. Spakman, P. Monié, B. Meyer, and R. Wortel (2011), Zagros orogeny: A subduction-dominated process, *Geol. Mag.*, *148*(5–6), 692–725, doi:10.1017/S001675681100046X.

Ahmadhadi, F., J.-M. Daniel, M. Azzizadeh, and O. Lacombe (2008), Evidence for pre-folding vein development in the Oligo-Miocene Asmari Formation in the Central Zagros Fold Belt, Iran: Fracture patterns within Asmari FM, Iran, *Tectonics*, *27*, TC1016, doi:10.1029/2006TC001978.

Anderson, E. M. (1942), *Dynamics of Faulting and Dyke Formation*, Oliver and Boyd, Edinburgh.

Angelier, J. (1984), Tectonic analysis of fault slip data sets, *J. Geophys. Res.*, *89*(B7), 5835–5848, doi:10.1029/JB089iB07p05835.

Angelier, J. (1990), Inversion of field data in fault tectonics to obtain the regional stress—III. A new rapid direct inversion method by analytical means, *Geophys. J. Int.*, *103*(2), 363–376.

Angelier, J., A. Tarantola, B. Valette, and S. Manoussis (1982), Inversion of field data in fault tectonics to obtain the regional stress—I. Single phase fault populations: A new method of computing the stress tensor, *Geophys. J. Int.*, *69*(3), 607–621.
Angiboust, S., P. Agard, J. C. M. De Hoog, J. Omrani, and A. Plunder (2013), Insights on deep, accretionary subduction processes from the Sistan ophiolitic "mélange" (Eastern Iran), *Lithos*, *156–159*, 139–158, doi:10.1016/j.lithos.2012.11.007.
Armijo, R., and A. Cisternas (1978), Un problème inverse en microtectonique cassante, *C. R. Acad. Sci. Paris*, *287*(D), 595–598.
Aubourg, C., B. Smith, A. Eshraghi, O. Lacombe, C. Authemayou, K. Amrouch, O. Bellier, and F. Mouthereau (2010), New magnetic fabric data and their comparison with palaeostress markers in the Western Fars Arc (Zagros, Iran): Tectonic implications, *Geol. Soc. London Spec. Publ.*, *330*(1), 97–120, doi:10.1144/SP330.6.
Authemayou, C., O. Bellier, D. Chardon, Z. Malekzade, and M. Abassi (2005), Role of the Kazerun fault system in active deformation of the Zagros fold-and-thrust belt (Iran), *C. R. Geosci.*, *337*(5), 539–545, doi:10.1016/j.crte.2004.12.007.
Authemayou, C., D. Chardon, O. Bellier, Z. Malekzadeh, E. Shabanian, and M. R. Abbassi (2006), Late Cenozoic partitioning of oblique plate convergence in the Zagros fold-and-thrust belt (Iran), *Tectonics*, *25*, TC3002, doi:10.1029/2005TC001860.
Babazadeh, S. A., and P. De Wever (2004), Early Cretaceous radiolarian assemblages from radiolarites in the Sistan Suture (eastern Iran), *Geodiversitas*, *26*(2), 185–206.
Bagheri, S., and G. M. Stampfli (2008), The Anarak, Jandaq and Posht-e-Badam metamorphic complexes in central Iran: New geological data, relationships and tectonic implications, *Tectonophysics*, *451*(1–4), 123–155, doi:10.1016/j.tecto.2007.11.047.
Ballato, P., C. E. Uba, A. Landgraf, M. R. Strecker, M. Sudo, D. F. Stockli, A. Friedrich, and S. H. Tabatabaei (2011), Arabia-Eurasia continental collision: Insights from late Tertiary foreland-basin evolution in the Alborz Mountains, northern Iran, *Geol. Soc. Am. Bull.*, *123*(1–2), 106–131, doi:10.1130/B30091.1.
Barrier, E., and B. Vrielynck (2008), Palaeotectonic map of the Middle East, Atlas of 14 maps, Tectonosedimentary-Palinspastic Maps from Late Norian to Pliocene., *Comm. Geol. Map World CCMW CCGM*.
Berberian, F., and M. Berberian (1981), Tectono-plutonic episodes in Iran, *Geodyn. Ser.*, *3*, 5–32.
Berberian, M., J. A. Jackson, M. Qorashi, M. M. Khatib, K. Priestley, M. Talebian, and M. Ghafuri-Ashtiani (1999), The 1997 May 10 Zirkuh (Qa'enat) earthquake (Mw 7.2): Faulting along the Sistan suture zone of eastern Iran, *Geophys. J. Int.*, *136*(3), 671–694.
Berberian, M., J. A. Jackson, M. Qorashi, M. Talebian, M. Khatib, and K. Priestley (2000), The 1994 Sefidabeh earthquakes in eastern Iran: Blind thrusting and bedding-plane slip on a growing anticline, and active tectonics of the Sistan suture zone, *Geophys. J. Int.*, *142*(2), 283–299.
Bergerat, F. (1987), Stress fields in the European plateform at the time of Africa-Eurasia collision, *Tectonics*, *6*(2), 99–132, doi:10.1029/TC006i002p00099.
Bott, M. H. P. (1959), The mechanics of oblique slip faulting, *Geol. Mag.*, *96*, 109–117.
Bröcker, M., G. Fotoohi Rad, R. Burgess, S. Theunissen, I. Paderin, N. Rodionov, and Z. Salimi (2013), New age constraints for the geodynamic evolution of the Sistan Suture Zone, eastern Iran, *Lithos*, *170–171*, 17–34, doi:10.1016/j.lithos.2013.02.012.
Calzolari, G., M. Della Seta, F. Rossetti, R. Nozaem, G. Vignaroli, D. Cosentino, and C. Faccenna (2016a), Geomorphic signal of active faulting at the northern edge of Lut Block: Insights on the kinematic scenario of Central Iran: Tectonic geomorphology in central Iran, *Tectonics*, *35*, 76–102, doi:10.1002/2015TC003869.
Calzolari, G., F. Rossetti, M. Della Seta, R. Nozaem, V. Olivetti, M. L. Balestrieri, D. Cosentino, C. Faccenna, F. M. Stuart, and G. Vignaroli (2016b), Spatio-temporal evolution of intraplate strike-slip faulting: The Neogene–Quaternary Kuh-e-Faghan Fault, central Iran, *Geol. Soc. Am. Bull.*, *128*(3–4), 374–396, doi:10.1130/B31266.1.
Camp, V. E., and R. J. Griffis (1982), Character, genesis and tectonic setting of igneous rocks in the Sistan suture zone, eastern Iran, *Lithos*, *15*(3), 221–239.
Carey, E. (1979), Recherche des directions principales de contraintes associees au jeu d'une population de failles, *Rev. Geogr. Phys. Geol. Dyn.*, *21*(1), 57–66.
Carey, E., and B. Brunier (1974), Analyse théorique et numérique d'un modèle mécanique élémentaire appliqué à l'étude d'une population de failles, *C. R. Acad. Sci. Paris*, *279*(D), 891–894.
Angelier, J. (1975), Sur l'analyse de mesures recueillies dans des sites faillés: l'utilité d'une confrontation entre les méthodes dynamiques et cinématiques, *C. R. Acad. Sci. Paris*, *281*, 1805–1808.
Delaloye, M., and J. Desmons (1980), Ophiolites and melange terranes in Iran: A geochronological study and its paleotectonic implications, *Tectonophysics*, *68*(1), 83–111.
Delvaux, D., R. Moeys, G. Stapel, C. Petit, K. Levi, A. Miroshnichenko, V. Ruzhich, and V. San'kov (1997), Paleostress reconstructions and geodynamics of the Baikal region, Central Asia, Part 2. Cenozoic rifting, *Tectonophysics*, *282*, 1–38.
Dercourt, J., et al. (1986), Geological evolution of the Tethys belt from the Atlantic to the Pamirs since the Lias, *Tectonophysics*, *123*(1), 241–315.
Dolati, A., and J.-P. Burg (2013), Preliminary fault analysis and paleostress evolution in the Makran Fold-and-Thrust Belt in Iran, in *Lithosphere Dynamics and Sedimentary Basins: The Arabian Plate and Analogues*, edited by K. Al Hosani et al., pp. 261–277, Springer, Berlin.
Dziewonski, A. M., T. A. Chou, and J. H. Woodhouse (1981), Determination of earthquake source parameters from waveform data for studies of global and regional seismicity, *J. Geophys. Res.*, *86*(B4), 2825–2852.
Eftekhar-Nezhad, J., and F. Vahdati Danesmand (1991), Geological map of Birjand 1:250 000 scale, *Geol. Surv. Iran*.
Etchecopar, A., G. Vasseur, and M. Daignieres (1981), An inverse problem in microtectonics for the determination of stress tensors from fault striation analysis, *J. Struct. Geol.*, *3*(1), 51–65.
Fabbri, O. (2000), Extensional deformation in the nortern Ryukyu arc indicated by mesoscale fractures in the middle Miocene deposits of Tanegashima Island, Japan, *J. Geol. Soc. Jpn.*, *106*(3), 234–243.
Farbod, Y., O. Bellier, E. Shabanian, and M. R. Abbassi (2011), Geomorphic and structural variations along the Doruneh Fault System (central Iran): Active faulting of the doruneh fault, *Tectonics*, *30*, TC6014, doi:10.1029/2011TC002889.
Farbod, Y., E. Shabanian, O. Bellier, M. R. Abbassi, R. Braucher, L. Benedetti, D. Bourlès, and K. Hessami (2016), Spatial variations in late Quaternary slip rates along the Doruneh Fault System (Central Iran): Quaternary slip rates along the doruneh fault system, *Tectonics*, *35*, 386–406, doi:10.1002/2015TC003862.
Fattahpour, V., and M. Moosavi (2010), Stress inversion from the focal mechanism solution of Bam earthquake aftershocks (Iran, 2003), *J. Geophys. Eng.*, *7*(3), 290–301, doi:10.1088/1742-2132/7/3/008.
Fauvelet, E., and J. Eftekhar-Nezhad (1990), Explanatory text of the Gazik quadrangle map 1:250,000.
Fotoohi Rad, G. R., G. T. R. Droop, S. Amini, and M. Moazzen (2005), Eclogites and blueschists of the Sistan Suture Zone, eastern Iran: A comparison of P–T histories from a subduction mélange, *Lithos*, *84*(1–2), 1–24, doi:10.1016/j.lithos.2005.01.007.
Fournier, M., P. Agard, and C. Petit (2008), Micro-tectonic constraints on the evolution of the Barles half-window (Digne nappe, Southern Alps). Implications for the timing of folding in the Valensole foreland basin, *Bull. Soc. Géol. Fr.*, *179*(6), 551–568.
Freund, R. (1970), Rotation of stricke slip faults in Sistan, Southeast Iran, *J. Geol.*, *78*, 188–200.

Gowd, T. N., and S. V. Srirama Rao (1992), Tectonic stress field in the Indian subcontinent, *J. Geophys. Res.*, *97*(B8), 879–888, doi:10.1029/91JB03177.

Homberg, C., J. C. Hu, J. Angelier, F. Bergerat, and O. Lacombe (1997), Characterization of stress perturbations near major fault zones: Insights from 2-D distinct-element numerical modelling and field studies (Jura mountains), *J. Struc. Geol.*, *19*(5), 703–718.

Javadi, H. R., M. R. Ghassemi, M. Shahpasandzadeh, B. Guest, M. E. Ashtiani, A. Yassaghi, and M. Kouhpeyma (2013), History of faulting on the Doruneh Fault System: Implications for the kinematic changes of the Central Iranian Microplate, *Geol. Mag.*, *150*(04), 651–672, doi:10.1017/S0016756812000751.

Javadi, H. R., M. Esterabi Ashtiani, B. Guest, A. Yassaghi, M. R. Ghassemi, M. Shahpasandzadeh, and A. Naeimi (2015), Tectonic reversal of the western Doruneh Fault System: Implications for Central Asian tectonics: Tectonic reversal of the western DFS, *Tectonics*, *34*, 2034–2051, doi:10.1002/2015TC003931.

Javidfakhr, B., O. Bellier, E. Shabanian, L. Siame, L. Léanni, D. Bourlès, and S. Ahmadian (2011a), Fault kinematics and active tectonics at the southeastern boundary of the eastern Alborz (Abr and Khij fault zones): Geodynamic implications for NNE Iran, *J. Geodyn.*, *52*(3–4), 290–303, doi:10.1016/j.jog.2011.02.005.

Javidfakhr, B., O. Bellier, E. Shabanian, S. Ahmadian, and A. Saidi (2011b), Plio–Quaternary tectonic regime changes in the transition zone between Alborz and Kopeh Dagh mountain ranges (NE Iran), *Tectonophysics*, *506*(1–4), 86–108, doi:10.1016/j.tecto.2011.04.013.

Karagaranbafghi, F., J. P. T. Foeken, B. Guest, and F. M. Stuart (2012), Cooling history of the Chapedony metamorphic core complex, Central Iran: Implications for the Eurasia–Arabia collision, *Tectonophysics*, *524–525*, 100–107, doi:10.1016/j.tecto.2011.12.022.

Karagianni, I., C. B. Papazachos, E. M. Scordilis, and G. F. Karakaisis (2015), Reviewing the active stress field in Central Asia by using a modified stress tensor approach, *J. Seismol.*, *19*(2), 541–565, doi:10.1007/s10950-015-9481-4.

Kargaranbafghi, F., F. Neubauer, and J. Genser (2011), Cenozoic kinematic evolution of southwestern Central Iran: Strain partitioning and accommodation of Arabia–Eurasia convergence, *Tectonophysics*, *502*(1–2), 221–243, doi:10.1016/j.tecto.2010.02.004.

Lacombe, O., F. Mouthereau, S. Kargar, and B. Meyer (2006), Late Cenozoic and modern stress fields in the western Fars (Iran): Implications for the tectonic and kinematic evolution of central Zagros: Stress fields in the Western Fars (Iran), *Tectonics*, *25*, TC1003, doi:10.1029/2005TC001831.

Lacombe, O., K. Amrouch, F. Mouthereau, and L. Dissez (2007), Calcite twinning constraints on late Neogene stress patterns and deformation mechanisms in the active Zagros collision belt, *Geology*, *35*(3), 263–266.

Lacombe, O., N. Bellahsen, and F. Mouthereau (2011), Fracture patterns in the Zagros Simply Folded Belt (Fars, Iran): Constraints on early collisional tectonic history and role of basement faults, *Geol. Mag.*, *148*(5–6), 940–963, doi:10.1017/S001675681100029X.

Lawrence, R. D., R. S. Yeats, S. H. Khan, A. Farah, and K. A. DeJong (1981), Thrust and strike slip fault interaction along the Chaman transform zone, Pakistan, *Geol. Soc. London Spec. Publ.*, *9*(1), 363–370, doi:10.1144/GSL.SP.1981.009.01.33.

Malekzade, Z., O. Bellier, M. R. Abbassi, E. Shabanian, and C. Authemayou (2016), The effects of plate margin inhomogeneity on the deformation pattern within west-Central Zagros Fold-and-Thrust Belt, *Tectonophysics*, doi:10.1016/j.tecto.2016.01.030.

Marrett, R., and R. W. Allmendinger (1990), Kinematic analysis of fault-slip data, *J. Struct. Geol.*, *12*(8), 973–986.

Mattei, M., F. Cifelli, G. Muttoni, A. Zanchi, F. Berra, F. Mossavvari, and S. A. Eshraghi (2012), Neogene block rotation in central Iran: Evidence from paleomagnetic data, *Geol. Soc. Am. Bull.*, B30479–1.

Mattei, M., F. Cifelli, G. Muttoni, and H. Rashid (2015), Post-Cimmerian (Jurassic–Cenozoic) paleogeography and vertical axis tectonic rotations of Central Iran and the Alborz Mountains, *J. Asian Earth Sci.*, *102*, 92–101, doi:10.1016/j.jseaes.2014.09.038.

McQuarrie, N. (2003), Cenozoic evolution of Neotethys and implications for the causes of plate motions, *Geophys. Res. Lett.*, *30*(20), 2036, doi:10.1029/2003GL017992.

Mercier, J. L., E. Carey-Gailhardis, M. Sebrier, S. Stein, J. L. Mercier, P. Hancock, and P. England (1991), Palaeostress determinations from fault kinematics: Application to the neotectonics of the Himalayas-Tibet and the Central Andes [and discussion], *Philos. Trans. R. Soc. London Math. Phys. Eng. Sci.*, *337*(1645), 41–52, doi:10.1098/rsta.1991.0105.

Moazzen, M., M. Modjarrad, and M. Zarrinkoub (2006), Mineral chemistry, petrogenesis and P–T conditions of formation of harzburgitic peridotites from south of Birjand, Eastern Iran, *J. Asian Earth Sci.*, doi:10.1016/j.jseaes.2005.07.009.

Mobasher, K., and H. A. Babaie (2008), Kinematic significance of fold- and fault-related fracture systems in the Zagros mountains, southern Iran, *Tectonophysics*, *451*(1–4), 156–169, doi:10.1016/j.tecto.2007.11.060.

Moghadam, H. S., H. Whitechurch, M. Rahgoshay, and I. Monsef (2009), Significance of Nain-Baft ophiolitic belt (Iran): Short-lived, transtensional Cretaceous back-arc oceanic basins over the Tethyan subduction zone, *C. R. Geosci.*, *341*(12), 1016–1028, doi:10.1016/j.crte.2009.06.011.

Mouthereau, F., O. Lacombe, and J. Vergés (2012), Building the Zagros collisional orogen: Timing, strain distribution and the dynamics of Arabia/Eurasia plate convergence, *Tectonophysics*, *532–535*, 27–60, doi:10.1016/j.tecto.2012.01.022.

Nabavi, M. H., and M. Shahrabi (1981), Geological map of Porang 1:100 000 scale; N° 8054, Geological Survey of Iran, Tehran.

Nadimi, A. (2007), Evolution of the Central Iranian basement, *Gondwana Res.*, *12*(3), 324–333, doi:10.1016/j.gr.2006.10.012.

Navabpour, P., and E. Barrier (2012), Stress states in the Zagros fold-and-thrust belt from passive margin to collisional tectonic setting, *Tectonophysics*, *581*, 76–83, doi:10.1016/j.tecto.2012.01.011.

Navabpour, P., J. Angelier, and E. Barrier (2007), Cenozoic post-collisional brittle tectonic history and stress reorientation in the High Zagros Belt (Iran, Fars Province), *Tectonophysics*, *432*(1–4), 101–131, doi:10.1016/j.tecto.2006.12.007.

Navabpour, P., J. Angelier, and E. Barrier (2008), Stress state reconstruction of oblique collision and evolution of deformation partitioning in W-Zagros (Iran, Kermanshah), *Geophys. J. Int.*, *175*(2), 755–782, doi:10.1111/j.1365-246X.2008.03916.x.

Nozaem, R., M. Mohajjel, F. Rossetti, M. Della Seta, G. Vignaroli, A. Yassaghi, F. Salvini, and M. Eliassi (2013), Post-Neogene right-lateral strike–slip tectonics at the north-western edge of the Lut Block (Kuh-e–Sarhangi Fault), Central Iran, *Tectonophysics*, *589*, 220–233, doi:10.1016/j.tecto.2013.01.001.

Pang, K.-N., S.-L. Chung, M. H. Zarrinkoub, S. S. Mohammadi, H.-M. Yang, C.-H. Chu, H.-Y. Lee, and C.-H. Lo (2012), Age, geochemical characteristics and petrogenesis of Late Cenozoic intraplate alkali basalts in the Lut–Sistan region, eastern Iran, *Chem. Geol.*, *306–307*, 40–53, doi:10.1016/j.chemgeo.2012.02.020.

Pang, K.-N., S.-L. Chung, M. H. Zarrinkoub, M. M. Khatib, S. S. Mohammadi, H.-Y. Chiu, C.-H. Chu, H.-Y. Lee, and C.-H. Lo (2013), Eocene–Oligocene post-collisional magmatism in the Lut–Sistan region, eastern Iran: Magma genesis and tectonic implications, *Lithos*, *180–181*, 234–251, doi:10.1016/j.lithos.2013.05.009.

Reches, Z. E. (1987), Determination of the tectonic stress tensor from slip along faults that obey the Coulomb yield condition, *Tectonics*, *6*(6), 849–861, doi:10.1029/TC006i006p00849.

Regard, V., O. Bellier, J.-C. Thomas, M. R. Abbassi, J. Mercier, E. Shabanian, K. Feghhi, and S. Soleymani (2004), Accommodation of Arabia-Eurasia convergence in the Zagros-Makran transfer zone, SE Iran: A transition between collision and subduction through a young deforming system: Collision-subduction transition in Iran, *Tectonics*, *23*, TC4007, doi:10.1029/2003TC001599.

Saccani, E., M. Delavari, L. Beccaluva, and S. Amini (2010), Petrological and geochemical constraints on the origin of the Nehbandan ophiolitic complex (eastern Iran): Implication for the evolution of the Sistan Ocean, *Lithos*, *117*(1–4), 209–228, doi:10.1016/j.lithos.2010.02.016.
Shabanian, E., O. Bellier, M. R. Abbassi, L. Siame, and Y. Farbod (2010), Plio-Quaternary stress states in NE Iran: Kopeh Dagh and Allah Dagh-Binalud mountain ranges, *Tectonophysics*, *480*(1–4), 280–304, doi:10.1016/j.tecto.2009.10.022.
Shafaii Moghadam, H., F. Corfu, M. Chiaradia, R. J. Stern, and G. Ghorbani (2014), Sabzevar ophiolite, NE Iran: Progress from embryonic oceanic lithosphere into magmatic arc constrained by new isotopic and geochemical data, *Lithos*, *210–211*, 224–241.
Stöcklin, J. (1968), Structural history and tectonics of Iran: A review, *Am. Assoc. Pet. Geol. Bull.*, *52*(7), 1229–1258.
Tapponnier, P., et al. (1981), The Tibetan side of the India-Eurasia collision, *Nature*, *294*(5840), 405–410, doi:10.1038/294405a0.
Tirrul, R., R. J. Griffis, and V. E. Camp (1980), Geology of the Zabol Quadrangle, 1: 250.000, *Rep*. *Submitt*. *Geol*. *Miner*. *Surv*. *Iran*, (180).
Tirrul, R., I. R. Bell, R. J. Griffis, and V. E. Camp (1983), The Sistan suture zone of eastern Iran, *Geol. Soc. Am. Bull.*, *94*, 134–150.
Vernant, P., et al. (2004), Present-day crustal deformation and plate kinematics in the Middle East constrained by GPS measurements in Iran and northern Oman, *Geophys. J. Int.*, *157*(1), 381–398, doi:10.1111/j.1365-246X.2004.02222.x.
Walker, R., and J. Jackson (2004), Active tectonics and late Cenozoic strain distribution in central and eastern Iran: Tectonics of Central and Eastern Iran, *Tectonics*, *23*, TC5010, doi:10.1029/2003TC001529.
Walker, R. T. (2006), A remote sensing study of active folding and faulting in southern Kerman province, S.E. Iran, *J. Struct. Geol.*, *28*(4), 654–668, doi:10.1016/j.jsg.2005.12.014.
Walker, R. T., and M. M. Khatib (2006), Active faulting in the Birjand region of NE Iran: Active faulting at Birjand in NE Iran, *Tectonics*, *25*, TC4016, doi:10.1029/2005TC001871.
Wallace, R. E. (1951), Geometry of shearing stress and relation to faulting, *J. Geol.*, *59*(2), 118–130.
Walpersdorf, A., D. Hatzfeld, H. Nankali, F. Tavakoli, F. Nilforoushan, M. Tatar, P. Vernant, J. Chéry, and F. Masson (2006), Difference in the GPS deformation pattern of North and Central Zagros (Iran), *Geophys. J. Int.*, *167*(3), 1077–1088, doi:10.1111/j.1365-246X.2006.03147.x.
Yamaji, A., S. Tomita, and M. Otsubo (2005), Bedding tilt test for paleostress analysis, *J. Struct. Geol.*, *27*(1), 161–170, doi:10.1016/j.jsg.2004.08.006.
Yazdi, S. H. M., M. Pourkermani, M. Arian, and A. Karkheiran (2012), Determination of stress orientation in Sabzevar ophiolite xone in (khorasan Razavi Province, Iran), *Indian J. Sci. Technol.*, *5*(10), 3500–3505.
Zamani, G., B. J. Angelier, and A. Zamani (2008), State of stress induced by plate convergence and stress partitioning in northeastern Iran, as indicated by focal mechanisms of earthquakes, *J. Geodyn.*, *45*(2–3), 120–132, doi:10.1016/j.jog.2007.07.003.
Zanchi, A., F. Berra, M. Mattei, M. R. Ghassemi, and J. Sabouri (2006), Inversion tectonics in central Alborz, Iran, *J. Struct. Geol.*, *28*(11), 2023–2037, doi:10.1016/j.jsg.2006.06.020.
Zarifi, Z., F. Nilfouroushan, and M. Raeesi (2014), Crustal stress map of Iran: Insight from seismic and geodetic computations, *Pure Appl. Geophys.*, *171*(7), 1219–1236, doi:10.1007/s00024-013-0711-9.
Zarrinkoub, M. H., K.-N. Pang, S.-L. Chung, M. M. Khatib, S. S. Mohammadi, H.-Y. Chiu, and H.-Y. Lee (2012), Zircon U–Pb age and geochemical constraints on the origin of the Birjand ophiolite, Sistan suture zone, eastern Iran, *Lithos*, *154*, 392–405, doi:10.1016/j.lithos.2012.08.007.
Zoback, M. L., and M. D. Zoback (1989), Tectonic stress field of the continental United States, *Geol. Soc. Am. Mem.*, *172*, 523–540.